Review

Zainab N. Jaf*, Hussein A. Miran, Zhong-Tao Jiang and Mohammednoor Altarawneh*

Molybdenum nitrides from structures to industrial applications

https://doi.org/10.1515/revce-2021-0002
Received January 16, 2021; accepted July 20, 2021;
published online August 23, 2021

Abstract: Owing to their remarkable characteristics, refractory molybdenum nitride (MoN_x)-based compounds have been deployed in a wide range of strategic industrial applications. This review reports the electronic and structural properties that render MoN_x materials as potent catalytic surfaces for numerous chemical reactions and surveys the syntheses, procedures, and catalytic applications in pertinent industries such as the petroleum industry. In particular, hydrogenation, hydrodesulfurization, and hydrodeoxygenation are essential processes in the refinement of oil segments and their conversions into commodity fuels and platform chemicals. N-vacant sites over a catalyst's surface are a significant driver of diverse chemical phenomena. Studies on various reaction routes have emphasized that the transfer of adsorbed hydrogen atoms from the N-vacant sites reduces the activation barriers for bond breaking at key structural linkages. Density functional theory has recently provided an atomic-level understanding of Mo–N systems as active ingredients in hydrotreating processes. These Mo–N systems are potentially extendible to the hydrogenation of more complex molecules, most notably, oxygenated aromatic compounds.

Keywords: binary nitrides; catalysts; density functional theory; hydrodesulfurization; hydrogenation.

***Corresponding authors: Zainab N. Jaf**, Department of Physics, College of Education for Pure Sciences – Ibn Al-Haitham, University of Baghdad, Baghdad 10071, Iraq; and **Mohammednoor Altarawneh**, Department of Chemical and Petroleum Engineering, United Arab Emirates University, Sheikh Khalifa bin Zayed Street, Al-Ain 15551, United Arab Emirates, E-mail: zainab.n.a@ihcoedu.uobaghdad.edu.iq (Z. N. Jaf), mn.altarawneh@uaeu.ac.ae (M. Altarawneh). https://orcid.org/0000-0002-2832-3886 (M. Altarawneh)
Hussein A. Miran, Department of Physics, College of Education for Pure Sciences – Ibn Al-Haitham, University of Baghdad, Baghdad 10071, Iraq
Zhong-Tao Jiang, Surface Analysis and Materials Engineering Research Group, College of Science, Health, Engineering and Education, Murdoch University, Murdoch, WA 6150, Australia

1 Introduction

Transition metal nitrides (TMNs) are refractory ceramic compounds exhibiting various fascinating properties, including a high melting, remarkable oxidation resistance against wear and corrosion, chemical inertness, and excellent electrical conductivity (Oyama 1996; Toth 2014). These extraordinary properties primarily originate from the unique electronic and geometrical structures of TMNs. Their geometries comprise a mixture of covalent (metal and nonmetal), metallic (metal–metal), and ionic (metal and nonmetal charged) bonds (Calais 1977). The strong covalent bonding between TM and N atoms has been exploited in a wide range of applications, such as high-temperature coatings that resist hostile conditions (elevated temperatures and pressures, catalysts, and solar selective surfaces) (Alexander and Hargreaves 2010; Giordano and Antonietti 2011; Ham and Lee 2009; Lengauer 2000; Levy and Boudart 1973; Mitterer et al. 2000; Zhang et al. 2003). Moreover, the nitrogen introduced into metal–metal bonds increases the bond distance from that of the parent metal in TMNs, providing them a unique crystal structure that has received considerable interest. Furthermore, the exclusive electronic properties of the resultant bonds result in high catalytic activities of TMTs, which is similar to those of noble metals such as Pt, Pd, and Ru.

The synthesis methods of nitride-based materials generally require high temperatures and long reaction times (Gregory 1999). The energy-intensive synthesis routes of nitride-containing compounds primarily stem from the high energy of dissociating the triple bond of nitrogen molecules (945 vs. 498 kJ mol^{-1} required for dissociating the double bonds of oxygen molecules) (Luo 2002). This high energy prevents nitrogen atoms from developing ionic bonds with electropositive elements. Overall, thermodynamic phenomena may explain the scarcity of nitrides and their greater propensity to form unique geometries than oxides or carbides (Gregory 1999). Molybdenum nitrides (MoN) are arguably the most discussed group in TMNs with diverse applications in catalysts and hard coating materials. Number of comprehensive reviews focus on the structures,

thermodynamics, bonding nature, synthetics methods, catalysis, and characterizations of nitride-based compounds (Chen 1996; Lengauer 2005; Wang et al. 1995). This review covers two main aspects of Molybdenum nitrides -based materials:

- The chemistry of molybdenum nitrides. This perspective covers structural properties, synthesis methods, and phase stability diagrams.
- Catalytic mechanisms involving molybdenum nitrides in various heterogeneous reactions. This perspective focuses on the governing reaction networks, operational conditions, products, and chemical conversions.

2 Structural properties of TMNs in general

The geometric and electronic aspects of TMNs have been extensively investigated and reported (Chen 1996; Johansson 1995; Oyama 1996). As is well known, nitrides of Groups III–XII (*d*-block elements) exhibit an intermediate transition state between metallic and interstitial nitrides as non-metal atoms diffuse into the metal lattice (Toth 2014). Row 1 metals (Ti, V, Cr, Mn, Fe, Ni, and Co) are termed *intermediate compounds*, whereas Rows 2 and 3 metals, including (Zr, Nb, and Mo) and (Hf, Ta, W, and Re), respectively, from the so-called *interstitial compounds*. The carbides are structurally distinct from oxides. In oxides (carboides), the anions (cations) are the larger atoms and the cations (anions) occupy the interstitial sites. However, in TMNs, the nitrogen atoms are randomly distributed in half of the octahedral interstices, whereas the metal atoms occupy the lattice sites of face-centered cubic (*fcc*), hexagonal close packed (*hcp*), or simple hexagonal structures (Chen 1996). These sites may also be occupied by carbon- or oxygen-forming carbonitride and oxynitride, respectively. Furthermore, Hägg (1931) suggested that when the radius ratio of the nonmetal to metal atoms is less than 0.59, the interstitial compound group typically possesses a B1–NaCl structure (Goldschmid 2013). Although TMNs assume simple crystal structures, they typically differ from those of their corresponding parent metals. For instance, the stable version of metallic Mo crystallizes in the body-centered cubic (*bcc*) phase; however, its analogous stable nitride (Mo_2N) exhibits an *fcc*-like structure as depicted in Supplementary Figure S1. These structural modifications between the parent metal and the nitrogen-containing transition metal are ascribed to electronic factors (Oyama 1996).

The predominant stoichiometries in the early transition metal nitrides are TMN and TM_2N (where TM denotes transition metal). However, later transition metals mainly adopt the TM_3N stoichiometry because the atomic size decreases across the groups. Consequently, the lattices of metals with a high group number cannot host interstitial nitrogen atoms in their close-packed (*cp*) or hexagonal close-packed (*hcp*) arrangements (Lee and Ham 2003; Sproul 1986).

3 Electronic properties

The number of valence electrons largely determines the distinctive properties of an element or compound (Lee and Ham 2003). In terms of the shape and ordering of the bands, the density of states (DOS) of TMNs follow the trend of their corresponding transition metals (Gogotsi and Andrievski 2012). In transition metals, the *d*-band starts to fill from Ru and Os to Pd and Pt. Furthermore, the catalytic properties of Group IV–VI TMNs are similar to those of Group VIII–X transition metals because both forms possess a similar *d*-band. As revealed by X-ray photoemission spectroscopy (XPS), the electronic structures of refractory TMNs strongly correlate with their properties (Greczynski et al. 2017; Höchst et al. 1982). (Brewer 1968) reported the thermodynamic properties of several crystalline transition metals based on the Engel-Brewer theories (Hume-Rothery 1968). Using the theory that combines the electronic and crystal structures of the *bcc* and *hcp* configurations with the spectroscopic data of gaseous transition metal atoms, it is suggested that the structure of a metal or substitutional alloy firmly depends on the *sp* electrons. In particular, the number of *sp* valence electrons per atom (e/a) determines the shape of the unit cell. Ratios of 1–1.5, 1.7–2.1, and 2.5–3 correspond to the *bcc*, *hcp* and *fcc* configurations, respectively. The valence electron concentration reportedly provides a detailed description of the mechanical properties of Group IV–XII nitrides, carbides, and carbonitrides with a salt-rock structure (Koutná et al. 2018). First-principles investigations of the electronic properties of bulk TMNs in Groups V and VI were first reported (Papaconstantopoulos et al. 1985). The energy separations in the DOSs of TMNs increase from the 3*d* to 5*d* nitrides (i.e., CrN→MoN→WN). Furthermore, the electronic DOSs in the valence and core states of TMNs are related to the covalency degree of their chemical bonding. Along the same line of enquiry, the low stability of the cubic MoN phase has been linked to the increased charge transfer from Mo-*d* electrons to N-*p*. The number of N-*p* electrons correlates with the stoichiometric ratio N/Mo (Lévy et al. 1999). Figure 1 displays the

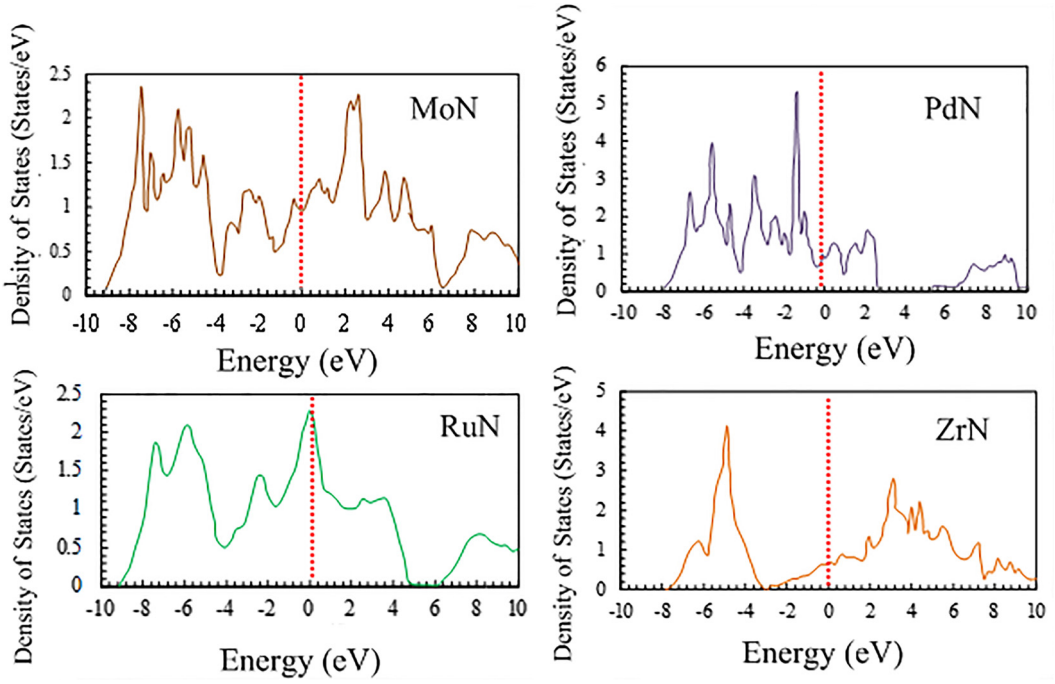

Figure 1: Theoretically predicted DOS of selected transition metal mononitrides. The Fermi energy level (denoted by the vertical dotted line) was arbitrarily set to zero (Zhao et al. 2010), reproduced with permission from Elsevier.

theoretically predicted DOSs of selected metal mononitrides. The absence of a band gap in the DOS curves indicates a metallic character (Zhao et al. 2010).

4 Mechanical properties

The hardness of a material reflects the material's resistance to different types of distortions (such as knocking or scratching). The hardness values of TMN compounds largely depend on their M/N ratios and reduce with increasing nitrogen contents. Hones et al. (2003) observed that *fcc* γ-Mo_2N has lower hardness than that of over-stoichiometric phases. The strength of the metal–nitrogen bonds in TMNs also contributes to their relative hardness. A decrease in hardness (i.e., elastic modulus) is mainly attributable to the diminishing covalent character of the bonding Ns. Under low nitrogen loads, the electrons in the low-lying bonding bands are only partially occupied, and the hardness increases. When the nitrogen contents increase, the low-lying bonding bands become fully occupied, the covalent bonds are broken, and the ionic bonds are weakened; accordingly, the hardness diminishes (Papaconstantopoulos et al. 1985).

Klimashin et al. (2016) thoroughly analysed the effect of N content and their vacancies on the mechanical properties of Mo–N coatings. Among all synthesized MoN_x configurations, the γ-$MoN_{0.53}$ displays the highest hardness of ~33 GPa. The valance electron concentration for this particular coating amounts to 8.6. This value reflects very well other VEC values for corresponding NaCl-like structures with the maximum hardness in other transition metal nitrides such as NbN_x and TaN_x (Jhi et al. 1999). In this regard, we propose that DFT-based mechanical properties can now be extrapolated to real scenarios of operational temperature and pressure through the quasi-harmonic approximation (QHA) approach. Thus, it will be insightful to re-assess the impact of nitrogen content on the stability of MoN_x coatings at elevated temperatures in light with published study (Klimashin et al. 2016). We have utilized the combined DFT-QHA approach to acquire volume-dependent thermo-elastic properties of two of the most investigated MoNx phases, namely, *c*-MoN and *h*-MoN (Jaf et al. 2016). Pertinent properties were obtained their melting point and a pressure of 12 GPa. We have established that the two structures of molybdenum nitride assume minor harmonic effects. This is affirmed by a negligible variation of considered thermo-mechanical properties with the increase of pressure and temperature. Similarly, Abdelkader et al. (2020) computed basic mechanical properties (including the elastic constant matrix) for the two tetragonal β-Mo_2N and cubic γ-Mo_2N phases

pointing out to the mechanically stability of the two nitrides. However, the former was predicted to incur higher thermodynamic stability.

Yu et al. (2016) argued that the recently synthesized *R*3*m* phase of MoN_2 at a modest pressure of 3.5 GPa to be thermodynamically and mechanically unstable. They examined the stable phase of MoN_2 by deploying the USPEX code. Two pernitride MoN_2 structures, namely hexagonal $P6_3/mmc$ and tetragonal $P4/mbm$, were deemed to be stable. The evaluated hardness values for hexagonal $P6_3/mmc$ and tetragonal $P4/mbm$ geometries amount to 22.3 and 32 GPa, respectively. These noticeably high values render these structures as potential candidates in the synthesis of hard coating materials. Moreover, the predicted elastic constants of MoN_2 $P6_3/mmc$ phase were extraordinarily high (C_{33} value of 952 GPa) close to that of diamond (C_{33} = 1079 GPa).

5 Molybdenum nitride phases

Nitrides of molybdenum possess several unique properties, including high hardness and superconducting temperature (Sangiovanni et al. 2011; Soignard et al. 2003). These properties have been exploited in diverse and niche fields. Among the applications of molybdenum nitrides are hard coatings for high-temperature machinery (Khojier et al. 2013; Suszko et al. 2005), diffusion barriers in microelectronic devices (Lee and Park 1996; Li et al. 2015), and enrichment of the tribological properties of hard coatings by forming the so-called Magnéli phase (Gassner et al. 2006). Technological applications of molybdenum nitrides greatly depend on their phases, which are themselves dictated by their nitrogen loads. Supplementary Table S1 enlists geometrical features of the MoN_x phases.

5.1 γ-$Mo_2N_{1\pm x}$ phase

The gamma phase (γ-Mo_2N) possesses an *fcc* structure with the $Fm\bar{3}m$ space group and a repeated ABCABC stacking sequence. This phase is stable at high temperatures, and the N atoms are randomly distributed (i.e., disordered) in half of the N octahedral sites (Jehn and Ettmayer 1978). The measured superconducting transition temperature T_c of this phase is 5.5 K (Wang et al. 2015a). Another phase γ-$Mo_2N_{1\pm x}$ presents an ordered array of vacancies with the $Pm\bar{3}m$ space group, which is distinguished from $Fm\bar{3}m$ by the presence of superstructure reflections (Tagliazucca et al. 2013). The Mo–N system crystallizes over a wide range of stoichiometries. In the fully stoichiometric geometry (i.e., the Mo:N stoichiometric ratio is 1:1), the Mo cations occupy an MoN_6 octahedral coordination environment. When the nitrogen sites are half-occupied (i.e., the Mo:N stoichiometric ratio is 2:1), the coordination number of Mo is reduced (Bull et al. 2004; Cao et al. 2015). Papaconstantopoulos and Pickett (1985) predicted that the fully stoichiometric configuration affords the maximum superconducting transition temperature (T_c ~ 30 K). This suggests that in the nonstoichiometric cubic structure $MoN_{0.5}$ formed by disordering the N atoms, the high-temperature superconductivity is affected by the reduced transition temperature. Figure 2a portrays the unit cell structure of the gamma phase.

5.2 β-Mo_2N phase

The β-Mo_2N phase is an ordered tetragonal structure with mechanical stability at low temperatures. This structure is often considered as a tetragonal adjustment of the cubic γ-Mo_2N phase with a doubled lattice constant *c* (forming the $I4_1/amd$ space group) (Karam and Ward 1970). The γ-Mo_2N phase transforms to β-Mo_2N at high temperatures. The synthesis routes and characterization of β-Mo_2N have been rarely reported (Ettmayer 1970). Inumaru et al. (2005) synthesized a crystalline phase of β-Mo_2N by pulsed laser deposition of molybdenum metal. X-ray diffraction (XRD) analysis revealed a composition of $Mo_2N_{0.85}$. The unit cell structure of this tetragonal phase is displayed in Figure 2b.

5.3 Metastable cubic B1-MoN

Although the stoichiometric cubic *B1*-MoN phase is thermodynamically unstable, it can be stabilized by carefully controlling the nitrogen concentration during synthesis (Jauberteau et al. 2015). The nitrogen amounts in MoN_x films is regulated from $Mo_1N_{0.5}$ to Mo_1N_1 by varying the growth rate (i.e., the N/Mo flux ratio) during the film deposition process. In a separate work, they synthesized an epitaxial B1-MoN_x ($0.98 < x < 1.03$) on α-Al_2O_3 by a thermal treatment below 650 °C (Inumaru et al. 2006b). A number of XRD studies have reported very similar lattice structures of the *NaCl*-Mo_2N phase with a = 4.16 Å (Shen 2003) and a = 4.151 Å (Kawashima et al. 2007). The stoichiometry of the B_1-MoN phase lies between those of $MoN_{0.5}$ and $MoN_{1.0}$. Any increase in nitrogen content is expected to enlarge the lattice parameter. The concentration of nitrogen vacancies primarily relies on the synthesis parameters, most notably, on the availability of nitrogen cations during sputtering (Inumaru et al. 2006a; Lin and Lai 2014) and the

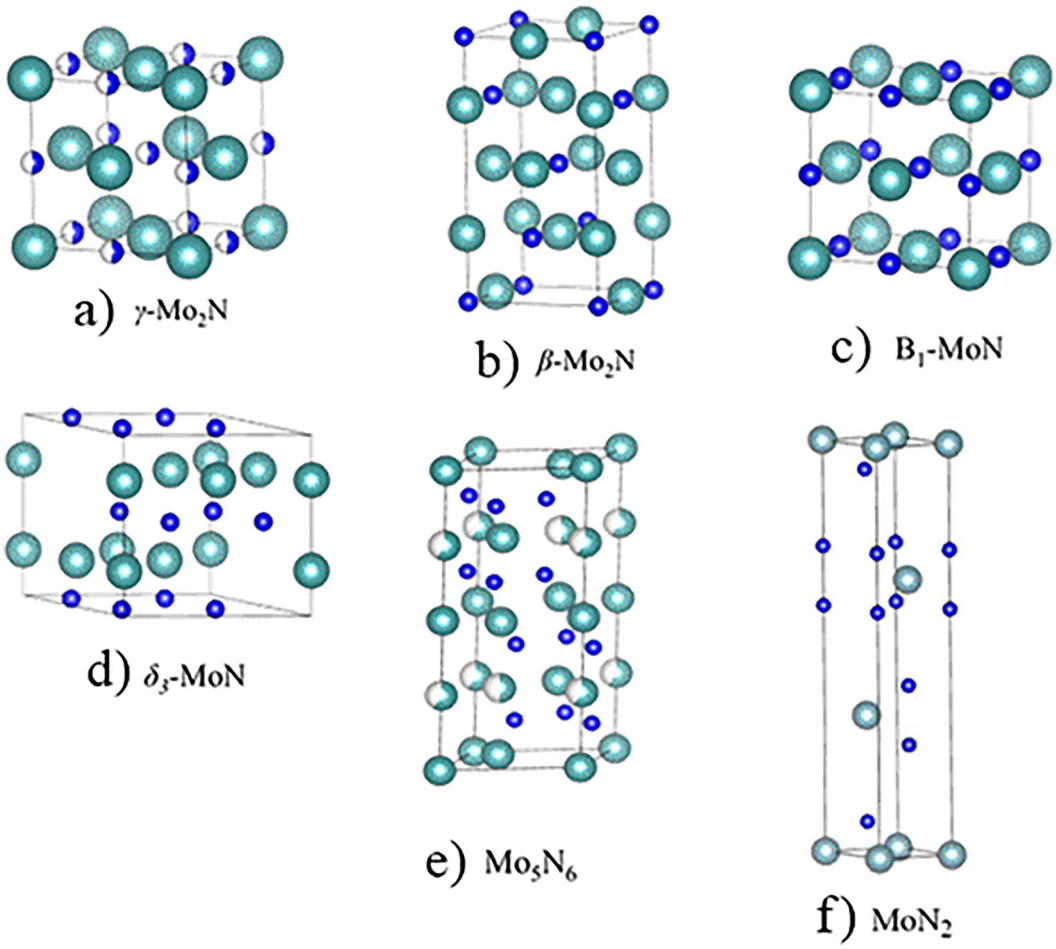

Figure 2: Phases of molybdenum nitrides (light blue spheres correspond to Mo atoms and blue spheres denote N atoms).

temperature treatments (Shen 2003). Figure 2c shows a unit cell with a *NaCl*-type structure.

In a comprehensive combined DFT-experimental investigation, Klimashin et al. (2016) presented relative stability diagrams for a wide spectrum of MoN structures. These structures were systematically generated using the special quasi-random structure (SQS) method. Based on computed formation energies, it was found that the WC-type δ_1-MoN_x and NiAs-type δ_2-MoN_x structures display similar formation energies for x resides in the vicinity of 0.85. Beyond this nitrogen content, the latter phase is energetically more preferred. In the cubic-structured NaCl-phases, configurations with N content close to 3:3 stoichiometry entails higher stability. DFT-based stability phase diagram by Klimashin et al. (2016) conveys two key remarks, First of all, the non-equilibrium technique of physical vapour deposition (PVD) can be fine-tuned to produce several metastable MoN_x structures. Second of all, the change in the nitrogen chemical potential drives a significant shift in the ordering stability of the MoN_x phases. However, it must be noted that the study of (Klimashin et al. 2016) utilized pure DFT functional whereas the presence of *d* orbitals in Mo atoms calls for the implementation of a more robust DFT + U methodology.

5.4 *δ*-MoN phase

The hexagonal δ-MoN configuration is arranged as metal layers with an ABAB staking sequence and a T_c of ~13.8 K (Wang et al. 2015a). Nonetheless, the positions of the N atoms cannot be unequivocally pinpointed, as the crystals are of poor quality (Bezinge et al. 1987). This phase has been fabricated by reduction of MoO_2 with NH_4Cl at high temperature (1773 K) under high NH_3 pressure (2 MPa) (Zhao and Range 2000). Bull et al. (2004) synthesized hexagonal δ_1-MoN via high temperature ammonolysis of $MoCl_5$. The produced crystals exhibited the $P6_3mc$ space

group with lattice constants of a = 2.87 Å and c = 2.81 Å. High-pressure ammonolysis affords the highly N-ordered hexagonal phase δ_3-MoN with nearly doubled lattice parameters (i.e., a = 5.73 Å and c = 5.61 Å). Ganin et al. (2006) fabricated several stoichiometric phases of hexagonal molybdenum nitrides by the plasma-enhanced chemical vapour deposition method and ammonolysis of $MoCl_5$ and MoS_2. The synthesised nitrides were called δ_1-MoN (*WC* type, $P\bar{6}m2$), δ_2-MoN (*NiAs*-type, $P6_3/mmc$), δ_3-MoN (*FeS*-type, $P6_3mc$), and nitrogen-rich phase (Mo_5N_6). The hexagonal δ-MoN phase demonstrated the highest bulk modulus among the Mo–N phases. Soignard et al. (2003) measured the bulk moduli of δ-MoN and γ-Mo_2N as 345 and 301 GPa, accordingly. The higher bulk modulus in δ-MoN is attributable to the high compressive stress. Figure 2d shows a unit cell of the hexagonal *WC*-type structure.

5.5 Mo_5N_6 phase

The Mo_5N_6 phase displays unequal layers of nitrogen prisms and octahedral-type arrangements along the c axis Figure 2e (Marchand et al. 1999). The nitrogen atoms form an AABB-type arrangement, analogous to the sulfur atoms in MoS_2. The molybdenum atoms saturate the trigonal prismatic sites and partially fill the octahedral sites. The Mo_5N_6 structure mimics the configurations of the *WC*- and *NiAs*-type building blocks, with partially filled Mo sites (Ganin et al. 2006).

5.6 Nitrogen-rich molybdenum

Figure 2f presents the geometrical unit cell of 3R-MoN_2. This cell features both a MoS_2-type structure and a rhombohedral $R3m$ arrangement. Wang et al. (2015b) produced a nitrogen-rich molybdenum nitride via the solid-state ion-exchange reaction under moderate pressure (3.5 GPa). Figure 3 shows the XRD patterns of different crystal structures of MoN and Mo_5N_6. XRD patterns of the synthesized 2D nitrogen-rich Mo_5N_6 nanosheets demonstrate various peak position that deviates from MoN. Suggesting that the extra (20%) nitrogen-incorporation significantly alters the crystal structure of conventional MoN (Jin et al. 2018).

Figure 4 depicts the structure and the DOS of the N-rich MoN_2 phase following a DFT investigation (Zhang et al. 2016). The MoN_2 assumes a hexagonal structure, with Mo and N atoms residing at two sites of a honeycomb lattice Figure 4a and b. Monolayers of MoN_2 comprises of atomic sheets stacked along the sequence N–Mo–N. As Figure 4c portrays, the MoN_2 exhibits a metallic character. We envisage that this profound catalytic activity of MoN_2 partially stems from this behaviour.

Similarly, Yu et al. (2016) explored the ground-state properties of bulk MoN_2 by DFT calculations. They proposed that the Mo atoms are sandwiched between N atoms. They also concluded (surprisingly) that the MoS_2-type MoN_2 structure proposed by (Wang et al. 2015b) is thermodynamically and mechanically unstable. This conclusion was supported by the negative elastic stiffness coefficients (C_{44}), multiple imaginary phonon frequencies, and positive enthalpy of formation. Using first-principles calculations, Wang and Ding (2016) inspected the structural stabilities and electronic properties of two-dimensional (2D) layered MoS_2-like molybdenum- and tungsten-dinitride nanosheets. They reported that contrary to the corresponding disulphide nanosheets, dinitride nanosheets of the MoN_2 phase contain durable soft modes that render them dynamically, thermally, and mechanically unstable. They also postulated that surface hydrogenation could effectively eliminate these soft modes. Hydrogenated MoN_2H_2 sheets as displayed in Supplementary Figure S2 are structurally stable and exhibit excellent electronic properties. A 2D transition metal dinitride sheet named tetra-MoN_2 possesses a significantly more stable ground-state geometry than the H–MoN_2 phase, along with a strain tenability that adjusts to the applied stress. Tetra-MoN_2 is a semiconductor with a band gap of only 1.41 eV (Zhang et al. 2017).

6 Phase stability diagram of the Mo–N system

Figure 5 represents a phase diagram of the Mo–N system proposed Jehn and Ettmayer (1978). In the α-phase, molybdenum hosts a nitrogen load ranging from 0 to 1.08 atomic weight (at.%). At temperatures below 1000 °C, the atomic-nitrogen concentration in α-Mo reaches 1.08 at.% at most, which is negligible. At 1860 °C and an equilibrium pressure of 670 atm, Mo can dissolve 1.08 at.% N (Jehn and Ettmayer 1978). In the 673–1123 K range, the cubic γ-Mo_2N phase is interchangeable with the tetragonal β-Mo_2N phase (Jauberteau et al. 2015). Gamma-phase Mo–N (γ-Mo_2N) is homogenous over a wide range of relative N ratios. This phase undergoes an ordering conversion between 400 and 850 °C (Lengauer 2000). The γ-Mo_2N phase appears at high temperatures as a defective B1-NaCl structure in which half of the nitrogen lattice positions are vacant sites. The nitrogen composition of this structure is around 27–35 at %. As discussed earlier, the B1-MoN phase can be produced

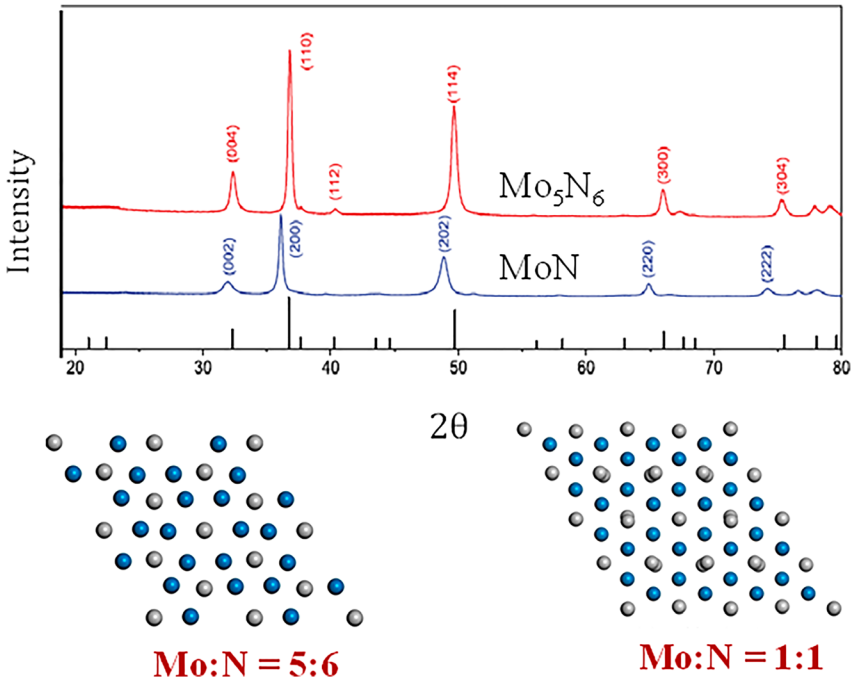

Figure 3: XRD patterns of Mo–M phases (Jin et al. 2018), reproduced with permission from the American Chemical Society, 2018.

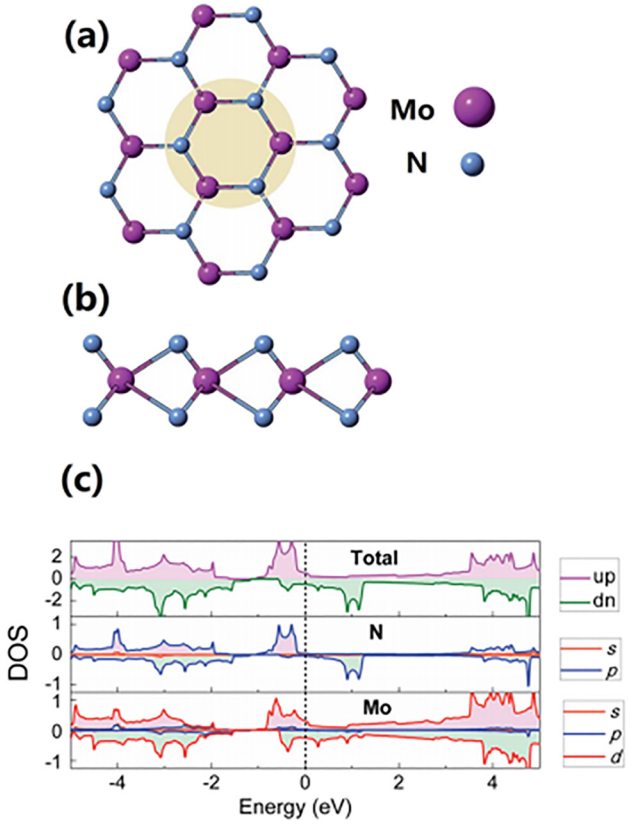

Figure 4: Top (a) and side (b) views of the MoN_2 phase and (c) its DOS curves (Zhang et al. 2016), reproduced with permission from the Royal Society of Chemistry.

by gradual filling of the vacant nitrogen sites in the defective γ-Mo_2N phase. This non-equilibrium phase readily transforms to the thermodynamically more stable hexagonal phase. Note that the thermodynamically unstable B1-MoN phase is absent in the stability diagram displayed in Figure 5, because it structurally rearranges into the hexagonal δ-MoN phase (Sanjinés et al. 1996). Saito and Asada (1987) concluded the same transformation sequence (γ-$Mo_2N \rightarrow$ B1-type MoN $\rightarrow \delta$-MoN) according to XRD spectra of the different phases. After implanting a nitrogen ion dose of 1×10^{17} ions/cm^2 into Mo thin films, they reported that the peaks corresponding to the *bcc*-Mo (110) and (200) directions were accompanied by new diffraction peaks belonging to the γ-Mo_2N phase. Under the maximum dose of 16×10^{17} ions/cm^2, the reflection peaks of the *bcc*-Mo crystal tended to vanish.

A more detail understanding pertinent to the effect of point defects in the stability ordering of MoN_x phases was firstly presented by Koutná et al. (2016) for cubic MoN and subsequently extended to include other structural configurations (Klimashin et al. 2016). Figure 6 depicts DFT-based phase diagram of Mo–N system (Koutná et al. 2016). The cubic Mo–N phase diagram corresponding to the stable compositions as a function of the N and Mo chemical potentials and the most stable structures corresponds to the structures with the lowest energy of formation E_f. As for the cubic phase, it was found that phases of cubic MoN

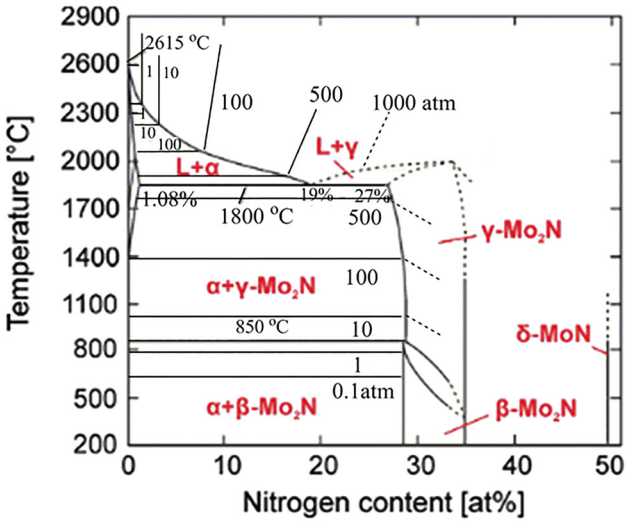

Figure 5: *T–P* phase stability diagram of the Mo–N system (Jehn and Ettmayer 1978), reproduced with permission from Elsevier.

with either vacant Mo or N sites exhibit similar formation energies for a vacancy concentration lower than 15%. The constructed phase diagram by Koutná et al. (2016) predicts the formation of four defect configurations ranging from

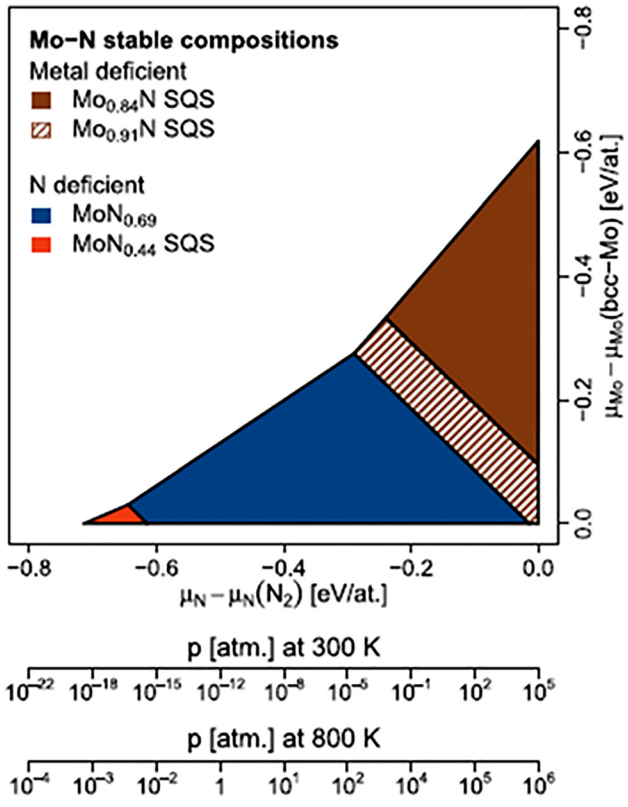

Figure 6: DFT- based phase diagram of Mo–N system as a function of the N and Mo chemical potentials (Koutná et al. 2018). The article was published as open access under the CC BY 3.0 license.

fully disordered to fully ordered configurations (namely $Mo_{0.91}N$, $MoN_{0.69}$, $MoN_{0.44}$, and $Mo_{0.84}N$). Herein, we propose that 3D stability diagram could be constructed for oxynitride phases analogously following the methodology pioneered by Koutná et al. (2016) and Klimashin et al. (2016). The underlying aim is to assess the combined effect of variation in N/O chemical potential and the potential emergence of metastable MoN_xO_y structures.

The dominant phase is affected not only by the *T–P* conditions but also by the amount of nitrogen in the system. Klimashin et al. (2016) theoretically and experimentally assessed the effect of nitrogen content and nitrogen vacancies on the geometries and mechanical properties of Mo–N thin films. The relative proportion of N-vacant sites alters the Mo–N bonding types and hence the relative thermodynamic hardness.

The elemental analysis, and hence the load of N vacant sites, were determined by energy dispersive X-ray spectroscopy (EDX) (Klimashin et al. 2016). The MoN_x phases were often examined through analysis of synchrotron X-ray data (Cao et al. 2015). High resolution transmission electron microscopy (TEM) images were also obtained for molybdenum nitrides with vacant sites (Guy et al. 2020) and display rows of hollow N sites. XPS spectra estimated the distribution of Mo oxidation states, and thus, highlighting the presence of N vacant sites (Choi et al. 1992). In typical XPS analysis (McGee and Thompson 2020), the ratio of N/Mo is attained on the basis decomposition of the Mo 3*p*3/2 and N 1*s* peaks. Along the same line of enquiry, the O/Mo ratios is computed based on the Mo 3*d*5/2 and O 1*s* peak areas. Neutron diffraction also is supremely suitable to investigate the N atom positions and site occupancy due to the large scattering length for nitrogen comparing to the molybdenum atoms implying that the bound coherent scattering cross sections of Mo and N are 5.7 and 11.01 b, correspondingly (Bull et al. 2006).

(Balasubramanian et al. 2017) coupled DFT calculations with the universal structure predictor evolutionary xtallography (USPEX) algorithm, an evolutionary phase-search algorithm that estimates the thermodynamic plausibility of Mo–N phases and their stoichiometries. The DFT–USPEX computations predicted eight thermodynamically stable molybdenum nitride phases with N-rich and N-deficient configurations: hexagonal δ-Mo_3N_2, cubic γ-$Mo_{11}N_8$, cubic γ-$Mo_{14}N_{11}$, orthorhombic ε-Mo_4N_3, monoclinic σ-MoN, σ-Mo_2N_3, tetragonal β-Mo_3N, and hexagonal δ-MoN_2. From the thermodynamic stability diagram shown in Figure 5, we note that stoichiometric and near-stoichiometric phases of N-atom ratios and occupancies adopt hexagonal-type structures, whereas nonstoichiometric phases adopt

different forms (B1-MoN, gamma γ-Mo_2N, tetragonal β-Mo_2N).

7 Morphologies of molybdenum nitride

Choi and Kumta (2011) fabricated nanocrystalline MoN_x powders (x = 0.77–1.32) at low temperature (≥600 °C) via NH_3 ammonolysis and nitridation of $MoCl_5$. The powders were intended for use as super capacitors. The γ-Mo_2N crystallites yielded the highest specific capacitance (111 F/g d at a scan rate of 2 mV/s). Combining experiments with DFT calculations. Xie et al. (2014) examined the hydrogen evolution reaction (HER) activity of 1.3 nm-thick hexagonal-phase MoN nanosheets synthesised by liquid exfoliation of bulk MoN materials. In the DFT calculations, the active sites of the atomically thin MoN nanosheets were identified as surface Mo atoms that catalyze the conversion of protons to hydrogen. By virtue of their rich surface-active sites and high conductivity, the MoN nanosheets delivered a high current density of 38.5 mA cm^2 at η = 300 mV. Joshi et al. (2017) synthesized micrometer-sized 2D nanosheets of hexagonal δ-MoN via a two-step process. The first step forms the 2D nanosheets from a MoO_3 precursor, and the second step transforms the oxide phase to the respective nitride through a reductive annealing process. Reduction of the oxide phase is accompanied by a phase transformation of the metal oxide to nitride, sulphide, or carbide in an NH_3, H_2S, or CH_4 environment, respectively. The formation mechanism of molybdenum nitride nanosheets was proposed by (Sun et al. 2018). They synthesized several phases of molybdenum nitride nanosheets (Mo_5N_6, δ-MoN, and γ-Mo_2N) by incorporating MoS_2 with nitrogen in a nanosheet configuration. Supplementary Figure S3 schematizes the possible reduction reactions of MoS_2 and NH_3. The occurring reaction is very sensitive to the working temperature. At 750 °C, Mo_5N_6 is generated directly with no immediate product. At 820 °C, Mo_5N_6 is synthesized by a one-step process and decomposes to δ-MoN when the MoS_2 is spent. At 950 °C, the only detected product is the δ-MoN phase. By gradual conversion of MoS_2, MoN decomposes first to γ-Mo_2N and later to a merging γ-Mo_2N plus β-Mo_2N phase. After complete consumption of MoS_2 at 1020 °C, the phase evolves as δ-MoN→ γ-Mo_2N→ β-Mo_2N→ Mo. At a higher temperature (1120 °C), only the β-Mo_2N intermediate eventually transforms into Mo.

8 Predictive modelling of the ground-state properties of the Mo–N system

Motivated by the growing need for reliable and representative data that can be utilized for shortlisting materials and tailoring their attributes toward a category of desired applications, many researchers have applied state-of-the-art computational methods to gain atomic-level insights into the potential applications and properties of Mo–N based materials. Powerful high-performance computational facilities have enabled the accurate modelling of materials. Researchers can now confirm the thermo-mechanical properties, lattice parameters, adsorption energies, XRD patterns, reaction rate constants, and turnover frequencies in models, most commonly by first principles calculations in the DFT framework. This section outlines the recent advances in DFT predictions of the bulk and surface properties of molybdenum nitrides. Stevens et al. (2006) investigated whether DFT models can accurately calculate the equilibrium bond lengths, dipole moments, and harmonic vibrational frequencies of Group VI (Cr, Mo, W) transition metals containing diatomic molecules. Using flexible basis sets, they examined a wide range of exchange-correlation functionals, and compared their results with analogous experimental measurements. The generalized gradient approximation (GGA) approach most accurately reproduced the experimental parameters. Isaev et al. (2007) investigated the ground state properties and phonon spectra of B1-type mononitrides of Group III–VI transition metals. The structural, elastic, and electronic properties of several MoN phases were investigated by (Kanoun et al. 2007) and are summarized in Table 1.

In DFT calculations, Zhao et al. (2010) reported the structural, mechanical, and electronic properties of 4-d transition-metal mononitrides with NaCl, NiAs, and WC-type structures. Among the investigated geometries,

Table 1: Computed and measured equilibrium lattice parameters: *a* (Å), *c* (Å), bulk modulus *B* (GPa), Young's modulus *E* (GPa), and Poisson's ratio *v*.

	NaCl–MoN	ZB–MoN	δ_1-MoN	δ_3-MoN	CsCl–MoN
a	4.304[a]	4.616[a]	2.868[a], 2.868[b]	5.710[a], 5.735[b]	2.67[a]
c	–	–	2.80[a], 2.81[b]	5.625[a], 5.628[b]	–
B	351.5[a]	274.8[a]	376.7[a]	379.4, 380[b]	354.8[a]
E	461.6[a]	139.6[a]	640.0[a]	611.3[a]	695.9[a]
v	0.23[a]	0.41[a]	0.24[a]	0.28[a]	0.13[a]

[a]DFT calculations by the GGA method (Kanoun et al. 2007). [b]Analogous experimental findings (Ganin et al. 2006).

the MoN phase with the NiAs-type structure displayed the highest hardness (with bulk and shear moduli of 351 and 239 GPa, respectively). Liu et al. (2014) conducted a DFT study of Group V–IIX transition metal nitrides. They reported that CrN, MoN and WN with the NbO structure exhibited the highest Vickers hardness (H_V > 20 GPa).

Several recent DFT studies predicted the existence of meta-stable MoN_x phases through extensive and systematic computational screening. Sun et al. (2017) employed a revolutionary data-mined structure-prediction algorithm (DMSP) to *in silico* synthesize new MoN_x structural phases. The procedure comprises several steps. It commenced with training the DMSP on the Inorganic Crystal Structure Database (ICSD) followed by isostructural mapping of potential compounds with the objective to pinpoint cations that are "statistically" susceptible for atomic substitution. Accurate identification of synthesizable MoN_x phases requires precise values of nitrogen chemical potential and enthalpies of formations of involved species. Through this extensive computational procedure, it has been predicted that stable structures of Mo_3N_5, and Mo_2N_3 at certain values of critical chemical potential of nitrogen (Sun et al. 2017). Most important, the DFT-powered scan procedure questioned the thermodynamic stability of the N-rich phase MoN_2 in view of its compositional proximity to that of MoN at accessible values of nitrogen chemical potential. While as the MoN_2 phase retains a stable phase evidenced by DFT calculations, the question arises on the governing mechanism for its formation. By using a similar global structural search approach to that of (Sun et al. 2017), Zhang et al. (2017) reached to the same conclusion; the MoS_2-like MoN_2 structure is not mechanically stable. They demonstrated that the ground state of the MoN_2 (termed as tetra-MoN_2 phase) exhibits a semi-conductor nature with higher stability than the metallic "seemingly unstable" H-MoN_2 phase. This new phase features a tuneable magnetism and Mo covalent bonding.

Wei et al. (2019) applied a crystal structure search algorithm to locate *R-3m* MoN_6 phase that is mechanically stable. This phase features a benzene-like N_6 structure that encircled isolated Mo cations (Figure 7). With the presence of N single bonds, Wei et al. (2019) predicted the phase to find direct applications in high-density-energy materials. Nonetheless, it was pointed out that this phase has not yet been synthesized experimentally. It will be insightful to use the DFT-scan approach to suggest synthesis mechanisms and a working nitrogen potential for this phase. A similar structural scan was performed by Ding et al. (2018). They located a stable orthorhombic *Cmc*21 MoN_2 configuration, which is even lower in energy than the experimental synthesized structure rhombohedral MoS_2-like MoN_2 structure. This finding is in accord with that of (Sun et al. 2017; Zhang et al. 2017).

DFT calculations can shed a light into the effect of synthesis conditions, most notably temperatures and nitrogen chemical potential, on the mechanical and electronic properties, and thermodynamic stability trends of the MoN_x phases. In this regard, a recent study by Lahmer (2019) found that creation of Mo vacancies entails lower formation energies under N rich conditions. On the contrary, formation of N vacant sites ensues via accessible energies with prevailing N poor conditions. Along the same line of enquiry, we postulate that the predictive power of

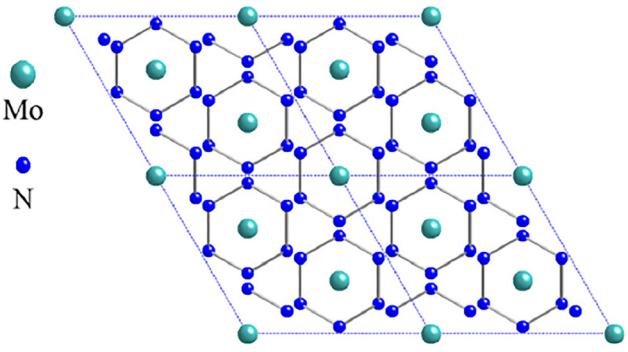

Figure 7: A top view of the predicted MoN_6 phase (Wei et al. 2019). Reproduced with permission from Elsevier.

DFT can be tailored to comprehend several intriguing aspects, such as:

- The effect of the dopants, N/Mo ratios and vacancies on the optical properties of MoN nano-sheets for applications in solar and optical devices.
- Mechanical properties of MoN-films with N/Mo and oxygen content vacancies under real P/T scenarios pertinent to their potential applications in hard coating materials.
- The interplay between the atomic constituents and a plausible electrochemical functionality of MoN-materials in supercapacitors.
- The role of surface N atoms and N vacant sites as adsorbents for molecules; germane to removal of pollutants in the aqueous phase.
- Structural stability of Mo_2N layers as a building block in the synthesis of MXenes stacking's with other metals.
- The global DFT-scan approach could be applied to design, based on a precise atomic-base scale, MoN_x materials with carefully manipulated catalytic properties and profound selectivity toward the formation of certain chemicals.

The combination between DFT calculations, structural search engines, and data mining are expected to enable ground-breaking discoveries in materials design a wide spectrum of applications. This is clearly underpinned by the superior benchmark accuracy of recent DFT functional that generally resides with a fraction of Å (for geometries) and a few meV (for energies) (Butler et al. 2019).

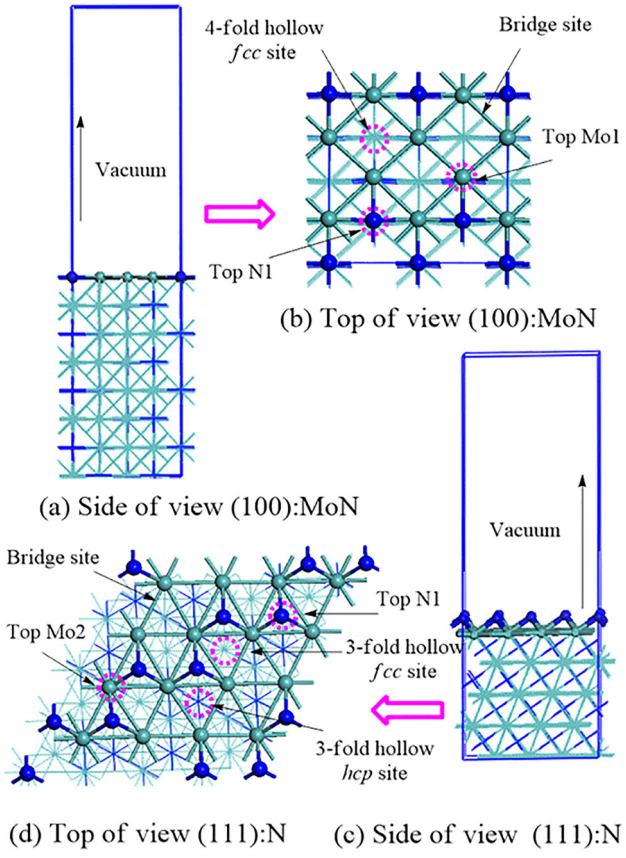

Figure 8: Optimised configurations of γ-Mo_2N (100): MoN and γ-Mo_2N (111): N-terminated surfaces and their possible adsorption sites. Light green, blue, and discretised pink circles denote molybdenum atom, nitrogen atoms, and surface active sites, respectively. Reproduced from (Altarawneh et al. 2016) with permission from the American Chemical Society, 2016.

9 γ-Mo_2N clean surfaces

Besides revealing the properties of bulk phases, DFT studies have provided the electronic and structural properties of Mo–N surfaces, most notably those of the γ-Mo_2N configuration. Surface relaxation, surface reconstructions relative to bulk positions and surface reaction rates have been most commonly reported. When cleaved along the three Miller indices, the optimized γ-Mo_2N bulk yields several configurations (Altarawneh et al. 2016). Some of these surfaces contain Mo/N mixed terminations while others present only N atoms in their topmost layers. Figures 8 and 9 portray optimized (i.e., minimal energy) structures of γ-Mo_2N surfaces and their potent active sites.

Figure 10 shows the phase stability diagram of molybdenum surfaces constructed in *ab initio* atomistic thermodynamics calculations. The most thermodynamically stable γ-Mo_2N surface, namely, γ-Mo_2N (111) has been subsequently targeted in several DFT-based studies on γ-Mo_2N catalysis (Altarawneh et al. 2016; Zaman 2010).

10 General synthetic routes of Mo–N catalysts via temperature-programmed reaction (TPR)

TMNs are typically synthesized at high temperature by metallurgical processes, yielding powders with low specific surface area (SSA) (Lee and Ham 2003). However, these powders are unsuitable for catalytic applications that require materials with high SSA. High-surface-area TMNs for catalytic applications are usually prepared by temperature-programmed reactions (TPRs) (Volpe and Boudart 1985). This section reviews the synthesis of transition metal nitrides, focusing on molybdenum nitride surfaces. In general, NH_3 is the preferred nitridation agent because it supplies nitrogens more easily than other nitrogen sources. The main synthetic methods of TMN catalysts are detailed elsewhere (Choi et al. 1994; Volpe

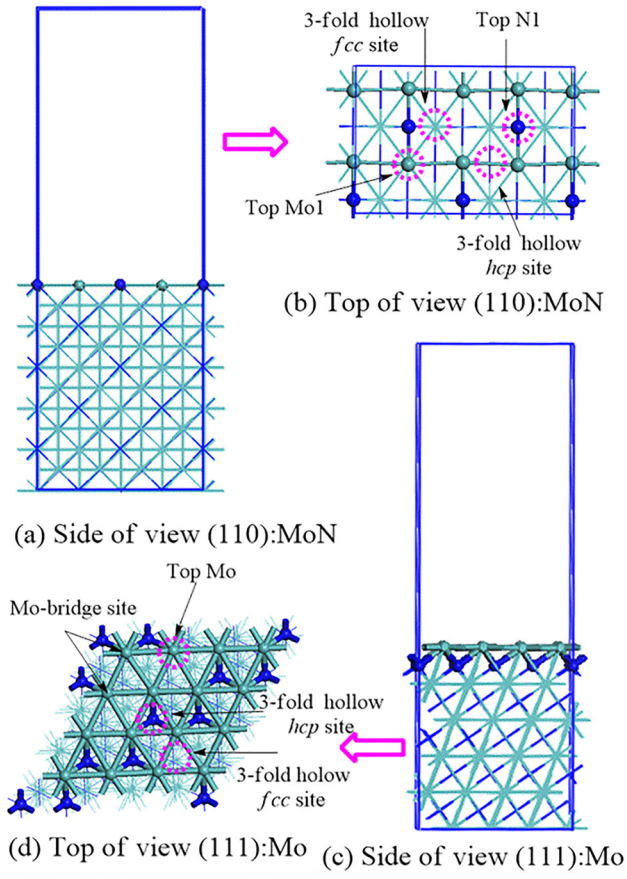

Figure 9: Optimised configurations of γ-Mo_2N (110): MoN and γ-Mo_2N (111): Mo- terminated surfaces. Light green, blue, and discretized pink circles denote molybdenum atoms, nitrogen atoms, and surface active sites, respectively. Reproduced from (Altarawneh et al. 2016) with permission from the American Chemical Society, 2016.

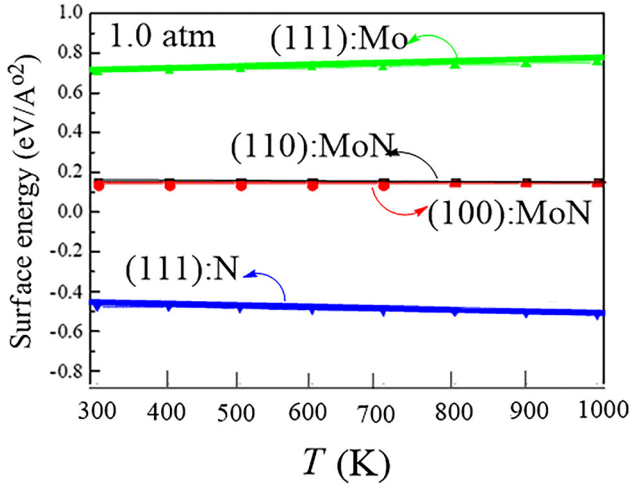

Figure 10: Phase stability diagram of molybdenum nitride surfaces. Reproduced from (Altarawneh et al. 2016) with permission from the American Chemical Society, 2016.

and Boudart 1985). TMNs are commonly fabricated by the gas–solid reaction between MO_3 (where M refers to Mo or W) and NH_3 or mixed NH_3 and Ar. Jaggers et al. (1990) proposed a reaction pathway yielding molybdenum nitride with a high surface area. They nitrided a MoO_3 precursor with NH_3, producing a mixture of MoO_xN_{1-x} and MoO_2. The oxynitride MoO_xN_{1-x} was then transformed to *fcc*-Mo_2N (at higher temperatures) and hexagonal MoN phases. However, the products of this direct nitridation method have low surface areas.

To realize the promising catalytic applications of MoN-based materials, researchers have increased the surface areas of these materials with modified synthetic methods (Mckay 2008). Volpe and Boudart (1985) reported the first synthesis of metal nitride catalysts with high surface area (220 m^2 g^{-1}), achieved by reacting NH_3 with a MoO_3 precursor. Electron diffraction measurements confirmed a topotactic N-induced conversion of the MoO_3 platelets. Marchand et al. (1996) documented that the morphology and surface area of the prepared nitride materials can be controlled by adjusting the NH_3 space velocity and operating temperature. The impact of the preparation parameters on the structural properties of synthesized catalysts was reported by Choi et al. (1994). They proposed a two-step heat treatment of molybdenum trioxide MoO_3 in an NH_3 atmosphere. In the first step, the temperature is increased from 623 to 723 K; in the second step, it is raised from 723 to 973 K. These two temperature processes occur at various space velocities. The results suggested that molybdenum nitride with high surface area forms by several reactions, which depend on the deployed space velocity and heating rates. They concluded that high-surface-area γ-Mo_2N resulted from the conversion of MoO_3 precursor into H_xMoO_3 and γ-$Mo_2O_yN_{1-y}$ intermediates. However, the reaction pathway via intermediates such as MoO_2 also produced molybdenum nitrides with medium and low surface areas. These categories of ammonolysis operations further promote the production of pseudo-morphic configurations (Mckay 2008). Temperature programmed ammonolysis is a widely applied technique to synthesis diverse phases of Mo–N based catalysts from different precursors (i.e., MoO_3, MoS_2 and $MoCl_5$) (Hargreaves 2013). The β-$Mo_2N_{0.78}$ phase is formed using N_2/H_2 as the synthesis gas with MoO_3 precursor. Moreover, MoS_2 and $MoCl_5$ δ-MoN with NiAs structure is formed while γ-Mo_2N displays a *fcc* structure. Whereas, the formation of both δ-MoN and Mo_5N_6 can be attained by ammonolysis of MoS_2 and $MoCl_5$.Typically, the formation temperature, which depends upon precursor, governed the final phase produced phase, suggesting β-MoN as the low temperatures phase and γ-Mo_2N as high

temperature phase while intermediate temperatures entails a mixture of the two phases (Hargreaves 2013).

Baek et al. (2021) has recently surveyed operational conditions that increases the surface area of molybdenum nitrides from nitridation of α-MoO_3 by ammonia. Investigated conditions spanned ammonia flow rate (2–11.5 L/h), temperature (425–846 °C), and heating rate (30–240 °C/h). It was found that a maximum surface area (~150 m^2/g) could be obtained at 630 °C. Higher temperature resulted in a phase transition γ-$Mo_2N \rightarrow \beta$-Mo_2N (at 770 °C) and to metallic Mo at 880 °C. Other optimum conditions constitute a molar NH_3 hourly space velocity at 64.2 L/h and a heating rate of 50 °C/h. More importantly, it was illustrated that the surface area is most sensitive to the nitridation temperatures. Other operational parameters exert rather a little variation. In preparation of high-surface β-Mo_2N catalysts from treatment of α-MoO_3 in N_2/H_2 stream, it is generally viewed that optimum conditions included a reaction temperature of 660–750 °C, a reaction time of 330 min, and a mixing ratio of 15% v/v N_2/H_2 (Cardenas-Lizana et al. 2011, 2013). As discussed earlier, the catalytic activities depend on the crystallographic phase structure and the availability of nitrogen vacant sites. For instance, in the gas phase hydrogenation of *p*-chloronitrobenzene (*p*-CNB) to *p*-chloroaniline (*p*-CAN) and through H_2 chemisorption/temperature programmed desorption analysis, a higher hydrogen uptake capacity (per unit area) was reported for tetragonal γ-Mo_2N (33–36 $m^2\ g^{-1}$) in reference to the cubic β-Mo_2N (7 $m^2\ g^{-1}$) (Perret et al. 2012). Haddix et al. (1988) characterized the adsorption of H_2 over γ-Mo_2N with high surface area (~120 $m^2\ g^{-1}$) by proton nuclear magnetic resonance (NMR). They proposed that H_2 strongly binds to the catalyst surface. Ranhotra et al. (1987) fabricated porous Mo_2N (*fcc*) powders by H_2 reduction of MoO_3 to metallic Mo in the presence of H_2. This phase contained pores of approximate diameter 17 Å, and exhibited a high Brunauer–Emmett–Teller (BET) surface area (180 m^2/g). More recently, Roy et al. (2015) prepared bulk γ-Mo_2N with a high surface area (116 $m^2\ g^{-1}$). In the programmed ammonolysis procedure, nitrided materials are typically cooled in inert gas (helium, argon or nitrogen) or in a diluted NH_3 atmosphere (Markel and Van Zee 1990). The nitrides are then passivated by passing through a dilute oxygen mixture (usually < 1%) in an inert gas (Colling et al. 1996; Furimsky 2003). Any formed oxide layer is then removed by reduction with H_2 or N_2/H_2. As is well documented, ammonolysis of $MoCl_5$ and MoS_2 precursors yields various nitrides, most notably, δ-MoN and Mo_5N_6 (Ganin et al. 2006). Wise and Markel (1994) synthesized a topotactic γ-Mo_2N with high surface area (150 $m^2\ g^{-1}$) via N_2/H_2 treatment of MoO_3. This nitridation procedure enables the facile elimination of heat transfer from the endothermic decomposition of NH_3 (the N–H bond dissociation energy of NH_3 is 93.21 kcal/mol (Luo 2002)). The surface area of a molybdenum nitride phase strongly depends on the synthesis conditions, namely, the flow rate of the nitrogen source, the temperature, and the heating rate. Li et al. (1998) synthesized a γ-Mo_2N by TPR. They proposed that the pseudo-morphological nature of the overall $NH_3 + MoO_3$ pyrolysis reaction increases the surface area of the final nitride phase. Claridge et al. (2000) produced nitrides from carbide precursors by a complex procedure that fabricates carbide and nitride materials with high surface area from binary and ternary oxide precursors (vanadium, niobium, tantalum, molybdenum, and tungsten). Typically, the TPR of various Mo–N and Mo–C phases from MoO_3 precursor. In various gas mixtures such as CH_4/H_2, C_2H_6/H_2, or NH_3, materials with surface areas exceeding 40 $m^2\ g^{-1}$ can be obtained (see Supplementary Figure S4).

Cairns et al. (2010) explored the influence of impurity level on the β-Mo_2N phase prepared by N_2/H_2 treatment of MoO_3 precursors. Minor loads (1.0 wt%) of Pd, Au, Ni, or Cu significantly altered the surface area of the β-Mo_2N phase obtained at 750 °C. In another study, Cairns et al. (2009) investigated the impact of precursor source on the β-Mo_2N phase. MoO_3 precursors supplied by different companies (AnalaR and Sigma–Aldrich, here labelled source A and source S, respectively) afforded β-Mo_2N phases with different morphologies (plate-like structures and deformed rectangular blocks from sources A and S, respectively, as evidenced in SEM images). Roy et al. (2015) developed a novel sacrificial support method for an alternative TPR of MoO_3 with an NH_3 nitrogen source. This method converts the MoO_2 intermediate using $MgMoO_4$, which is advantageous. Xu et al. (2015) suggested a synthetic approach called the self-assembly method, which fabricates a hexagonal-like MoN hierarchical nanochex from single-crystal nanowires.

11 Catalysis by molybdenum nitrides

Catalysis by metal nitrides relies on the presence of N-vacant sites and electronic structures that mimic those of Pt-based catalysts. In hydrogenation reactions of γ-Mo_2N, the N-vacant sites host the dissociated hydrogen atoms. The weakly bounded surface H atoms migrate to the adsorbed hydrocarbon species via relatively facile reactions. The governing catalytic reactions mapped in DFT studies are rather limited. Experimental studies on

Table 2: Summary of catalytic activities over various configurations of molybdenum nitride.

Catalyst	Preparation method	Shape and morphology	Surface area	Reaction products	Applications	Catalytic activity	References
γ-Mo_2N	TPR of MoO_3 with NH_3	Spherical and cubic particles	100 $m^2\ g^{-1}$	–	Pyridine hydro-denitrogenation catalysts	–	Choi et al. (1992)
Mo_2N	TPR of MoO_3 in N_2/H_2 treatment at 573 K, pressure of 5 MPa	–	9–115 $m^2\ g^{-1}$	Phenol	Hydrodeoxygenation (HDO) of guaiacol	10% conversion of guaiacol	Ghampson et al. (2012)
γ-Mo_2N	TPR NH_3	–	150 $m^2\ g^{-1}$	Ammonia	NH3 synthesis	Reaction rate at 673 K under 0.1 MPa was 43 μ mol $h^{-1}\ g^{-1}$	Kojima and Aika (2001)
Mo_2N/graphite	TPR of carbon-supported Mo precursors with NH_3	–	91 $m^2\ g^{-1}$	Unsaturated alcohol	Crotonaldehyde hydrogenation	High selectivity to unsaturated alcohol; crotylalcohol selectivities exceed 60%	Balasubramanian et al. (2018)
γ-Mo_2N	TPR reduction of MoO_3 in flowing NH_3	Porous particles	108 $m^2\ g^{-1}$	Butane	Thiophene hydro-desulfurization (HDS)	38.1% conversion efficiency at 673 K	Markel and Van Zee (1990)
$NiMoN_x$/C	Treatment of NiMo/C in NH3 flow at 700 °C	Nanosheets	–	–	Hydrogen evolution reaction (HER)	78 mV at 0.24 mA cm^{-2} in acid	Chen et al. (2012)
Mo_2N	TPR of MoO_3 with a mixture of N_2/H_2 gases	–	165 $m^2\ g^{-1}$	Methane	Hydrogenation of CO	High activity and selectivity of methane formation	Liu et al. (2003)
β-Mo_2N	Temperature programmed treatment of MoO_3 in flowing $N_2 + H_2$	Platelets	17 $m^2\ g^{-1}$	*p*-chloroaniline	Hydrogenation of *p*-chloronitrobenzene	100% selectivity towards NO_2 group reduction; reaction rate constant $k = 2.0\ min^{-1}$	Cardenas-Lizana et al. (2011)

Mo–N based catalysts have provided the chemical conversion values and surface characteristics of adsorbed species. The near-surface structures and compositions of a series of molybdenum nitride catalysts can be detected by high-resolution transmission electron microscopy combined with Fourier analysis, NMR measurements, and XPS (Furimsky 2003). Dongil (2019) recently reviewed the synthesis methods and catalytic properties of mono, binary, and ternary metal nitrides, and discussed the effect of the promoter on improving the catalytic performance. Table 2 stated the main catalytic activities over various configurations of molybdenum nitride.

12 Adsorption and activation of simple molecules

Molybdenum nitride compounds display high catalytic performance in a wide array of chemical reactions, including CO hydrogenation, ethane hydrogenolysis, NO reduction, and hydro-treatment processes. The availability of potent active sites on the catalyst surface critically affects the catalytic activity of a material. A catalytically potent material must adsorb and activate the commonly deployed probe molecules such as CO, H_2, NO, NH_3, C_5H_5N, and O_2. Kinetically, the activation route will close if the molecular adsorption and activation are slower than the surface-mediated reactions. To avoid deactivation or positing of the active sites, the produced radicals must be rapidly desorbed. When the products are desorbed from the surface, the active sites become available for another adsorption–activation–transfer–desorption cycle.

12.1 Hydrogen (H_2)

Catalysis on metal nitride surfaces is most commonly probed using hydrogen molecules. Typically, a catalyst is active when it can adsorb and activate molecular hydrogen (H_2) at a sufficient reaction rate for a proposed period of time within a specific temperature window. Hydrogen

adsorption over polycrystalline γ-Mo_2N commences sluggishly at room temperature, indicating a controlling resistance either in the film or at the pores (Li et al. 1996b). Supplementary Figure S5 plots the hydrogen uptakes of Mo_2N at 673 K (Li et al. 1996b). They measured the volumetric H_2-uptake over Mo_2N with a surface area of 79 $m^2\,g^{-1}$ during reduction at 673 K. As inferred by the uptake isotherms in the 308–623 K range, the total and reversible hydrogen uptakes increased with temperature. However, the irreversible hydrogen uptake was abruptly augmented when the uptake temperature reached 423 K. The irreversible hydrogen uptake was maximized at 473 K. One proposed mechanism of hydrogen adsorption signifies the heterolytic dissociation on the surface Mo–N pairs.

Based on NMR measurements, Haddix et al. (1988) concluded that hydrogen dissociatively adsorbs over γ-Mo_2N with a high surface area (~120 m^2/g). The total hydrogen uptake is upper-limited to approximately 10% of the total available BET surface area of γ-Mo_2N, suggesting a relatively high activation energy of the hydrogen molecules on γ-Mo_2N. The preferred adsorption sites were predicted as nitrogen-deficient sites. The interactions of H_2 and NH_3 with clean Mo(100) and nitrided Mo(100)-c(2 × 2)N surfaces were investigated via temperature programmed desorption (TPD) and Auger electron spectroscopy (Bafrali and Bell 1992). For a given hydrogen coverage, the H_2 concentration on the nitrided surface was ~4–10 times lower than the expected H_2 concentration on a clean Mo (100) surface. Li et al. (1996a) treated γ-Mo_2N with high surface area (134 m^2/g) in a hydrogen environment at specific temperatures. Prior to TPD experiments, the heat-treated samples were cooled to room temperature in an H_2 flow.

Via applying temperature programmed desorption (TPD) and temperature programmed adsorption (TPA) techniques (Zhang et al. 1997), it was found that the adsorbed hydrogen species migrated from sites with low adsorption energy (N-vacant sites) to sites with high adsorption energy (N-occupied sites). This facile surface diffusion sustains the dynamic equilibrium. Two hydrogen adsorption peaks appear at relatively high temperatures, one at 517 K and the other at 736 K, were detected, which were assigned to low and high adsorption sites, respectively. The TPD and TPA measurements indicated a rapid equilibrium between the adsorption and desorption reactions. It has been conveyed that Mo nitrides can straightforwardly chemisorb hydrogen owing to the contraction of the *d*-band and the changes in the electron density that result of the interstitial incorporation of N in the Mo metal lattice. Moreover, in the Mo_2N-based catalysts, hydrogenation reaction occurs over nitrogen deficient surface sites and Mo/N ratio influences the catalytic performance (Dongil 2019). Jaf et al. (2017) determined the molecular hydrogen adsorption behaviour over γ-Mo_2N in DFT calculations. It was demonstrated that hydrogen dissociation preferentially occurs over N vacant sites. Surface-assisted rupture over surface N sites ensues with significantly higher barriers. The H_2 adsorption and dissociation modes are portrayed in Figure 11 (Jaf et al. 2017).

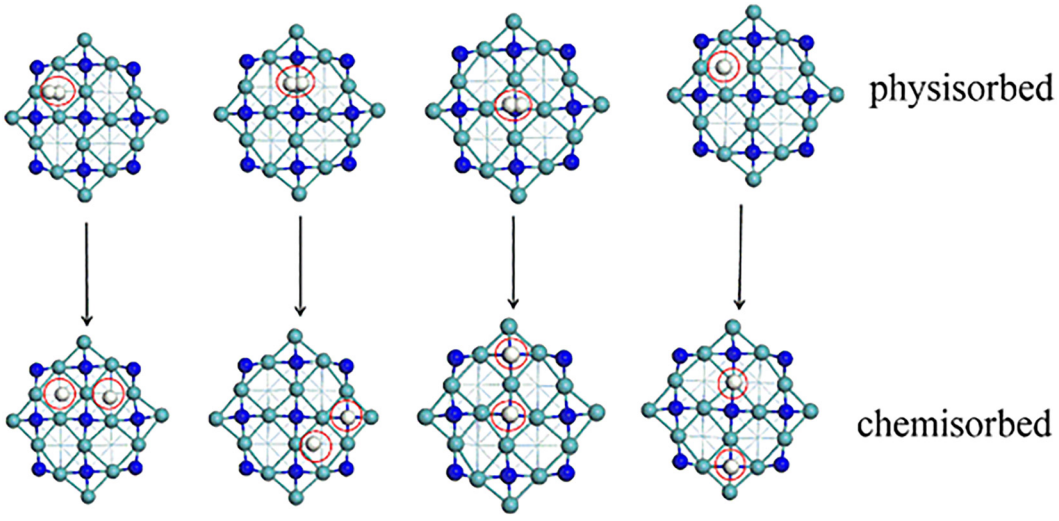

Figure 11: Non-dissociative and dissociative uptakes of molecular H_2 over the γ-Mo_2N (100) plane (top view), redrawn from (Jaf et al. 2017).

12.2 Oxygen (O_2)

Oxygen can reportedly diffuse into the subsurface layers of molybdenum nitrides. In a dilute O_2 mixture, a thin oxide passivating layer may form on the molybdenum nitride layer. The rates of subsurface oxygen diffusion and reaction with Mo are accelerated at higher temperatures. If subsurface oxygen diffusion occurs, higher operating temperatures can systematically enhance the overall uptake of oxygen because additional oxygen atoms can be adsorbed on subsurface sites (Choi et al. 1992). As shown in Supplementary Figure S6, the oxygen uptake is higher at 298 K than that at 195 K. This result can be explained by either the oxidation of subsurface layers or incomplete surface coverage. Markel and Van Zee (1990) demonstrated that the developed passivation layer produces an oxynitride phase but no distinct oxide phase.

Adsorption of oxygen on pure molybdenum surfaces results in the formation of oxynitride phases or a surface oxide layer. A recent study by Zhang et al. (2020) closely examined the role of the MoO_x oxide layer on the activity of Pt/γ-Mo_2N catalysts in the water-gas shift (WGS) reaction. Their kinetic analysis discloses that MoO_x ($2 < x < 3$) actually constitutes the intrinsically active surface in the Pt/γ-Mo_2N catalyst. Based on DFT computations, they explained that oxygen vacancies could readily form over the highly distorted MoO_x phases, and thus facilitating dissociative adsorption of water molecules. Along the same line of enquiry, it was shown that the acid-base character of O–Mo_2N surfaces strongly depends on the N/O atomic ratio (McGee and Thompson 2020). O–Mo_2N surfaces with the highest N/O atomic ratio entails the highest base site density, and hence selectivity toward the formation of certain products. Clearly, more studies are needed to better understand the interplay between the different atomic constituents, strain and defects, in the heterostructured Mo–O/N structures.

While the N vacant sites in metal nitrides assume some similar roles to the O vacant sites in transition metal oxides, there are some fundamental differences in their catalytic capacity. The surface unsaturation on both metal nitrides and oxides render the N/O vacant sites to act as a potent host for incoming gas phase molecules. Over transition metal oxides, the surface unsaturation is compensated by a reaction with water leading to tailored acid–base and redox properties. The redox reactions in transition metal oxides (as in ceria for instance) is derived by a relatively facile removal of surface oxygen leading to vacant sites (Wang et al. 2018). Similarly, it was reported via analysis of formed N species with different N isotopes (14 and 15) during de-NO_x reactions, that N vacant sites can be created through the removal of surface N atoms as nitrogen molecules from the γ-Mo_2N surface (He et al. 2001). Our computed overall energy penalty for the creation of N sites, on the γ-Mo_2N surface, amounted to 38.1 kcal/mol (Altarawneh et al. 2016). In hydrogenation reactions in particular, dissociated hydrogen atoms in transition metals resides over O sites rather than over vacant sites. In case of γ-Mo_2N surface Jaf et al. (2017), we have established that hydrogen atoms preferentially occupy N vacant sites rather than surface N sites.

12.3 Carbon monoxide (CO)

(Yang et al. 1998) investigated the surface active sites and adsorption properties of CO on fresh and reduced passivated samples of Mo_2N/Al_2O_3. The infrared (IR) spectra of CO adsorption over the fresh and reduced passivated samples exhibited distinct patterns. As presented in the IR spectrum of the fresh sample, the CO molecules adsorbed on the molybdenum and nitrogen sites, forming surface CO and NCO species. However, the reduced passivated sample formed an oxynitride layer. In general, the adsorbed CO molecules were dissociatedly adsorbed to C and O atoms. The IR results clearly demonstrated that the H_2 preadsorbed on fresh Mo_2N/Al_2O_3 hindered the CO adsorption, presumably by competing for the active sites.

In DFT calculations, Frapper et al. (2000) determined the most favorable energetic sites for CO molecular adsorption over the γ-Mo_2N (100) plane. The CO molecules were located at several adsorption sites. As shown in Figure 12, the four lowest-energy adsorption positions were Mo_1, Mo_2, surface N atoms, and 4-fold vacant sites. With an adsorption energy of –1.49 eV (–34.3 kcal/mol), the 4-fold vacant site was predicted to minimize the coordination mode. The adsorption energies were comparable at the three sites. Chemisorbed CO molecules on the Mo_2N catalyst have not been observed in experiments; however, in the IR interpretation, 4-fold hollows on the (100) *fcc* surface are promising active sites for diatomic molecules. The binding energies at the Mo_1 and Mo_2 sites were computed as –1.43 eV (–32.9 kcal/mol) and –1.32 eV (–30.4 kcal/mol), respectively (see Figure 12), similar to the adsorption energy of CO over Pd(100) (1.44 eV or 33.2 kcal/mol). This result demonstrates the well-known Pt-like catalytic properties of nitride molybdenum catalysts (Eichler 2002). CO adsorption over N sites yields chemisorbed NCO species with a slightly endothermic adsorption energy (0.23 eV or 5.3 kcal/mol); however, no activation barrier was reported.

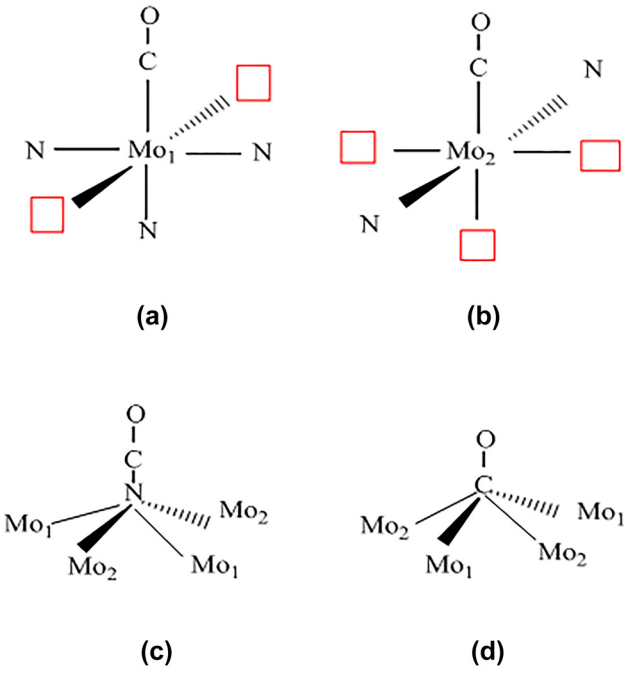

Figure 12: Schematic showing the possible active sites of CO adsorption on a clean (100) 1×1 surface: (a) on Mo_1, (b) on Mo_2, (c) on nitrogen surface atoms N_{surf}, and (d) on 4-fold sites μ_4-CO. Red squares symbols represent the vacant 4-fold hollow sites (Frapper et al. 2000). Reproduced with permission from the American Chemical Society.

Despite the low endothermicity, removal of surface N atoms is expected to encounter a sizable energy barrier (Frapper et al. 2000).

12.4 Adsorption of N_2

N_2 dissociatively adsorbs over Mo_2N and saturates the surface at high temperatures. In DFT calculations, the dissociation energy was predicted to be –2.04 eV/N_2 molecule (Frapper et al. 2000). Along the same line of enquiry, Hillis et al. (1966) predicted an extremely weak adsorption of molecular nitrogen over a molybdenum dioxide (MoO_2) surface during NH_3 synthesis. Moreover, 146 mL (STP)/(3.39-g molybdenum) of N_2 was absorbed on molybdenum metal subsequent to 69 h of nitridation in a pure N_2 atmosphere (Stampfl 2005). The chemisorption of nitrogen sites by nitrogen atoms over active metal–N bonds promotes the Mars–Krevelen mechanism (Jaf et al. 2018b). Molybdenum containing ternary nitrides such as Co_3Mo_3N will likely act as nitrogen transfer agents via the Mars–van Krevelen-like mechanism in the cyclic release and replenishment of nitrogen. In these reactions, Co_3Mo_3N serves as a nitrogen-storage medium (Hunter et al. 2010; Zeinalipour-Yazdi et al. 2015).

13 Catalytic activity of molybdenum nitride compounds

Several researchers have evaluated the catalytic performance of Group V and VI metal nitrides and carbides in catalyzing various reactions, including butane dehydrogenation, isomerization, and hydrogenolysis. Neylon et al. (1999) observed that the estimated turnover frequencies of nitride and carbide catalysts were of the same order of magnitude as that of the Pt–Sn/Al_2O_3 catalyst. Supplementary Figure S7 presents the Arrhenius plots of HER over selected Group V and VI metal nitrides and Pt–Sn/Al_2O_3. The molybdenum, tungsten, and vanadium nitrides were considerably active during a number of reactions. Herein, we solely focus on Mo_2N-mediated reactions as Table 2 demonstrates.

13.1 Hydrotreatment reactions

Hydrotreatment reactions are among the most essential catalytic processes in petrochemical industries. These reactions remove metals or heteroatoms such as, S, N, and O from crude oil feedstock. Depending on the target molecule and its atomic constituents, hydrogenation can be catalyzed by hydrodesulfurization (HDS), hydrodenitrogenation (HDN), hydrodeoxygenation (HDO), or hydrodemetallization (HDM) (Bafrali and Bell 1992; Furimsky 2003; Hillis et al. 1966). To limit the environmental damage caused by the increasing SO_x and NO_x emissions from thermal processes, strict rules and regulations have been imposed. Accordingly, catalyst scientists have turned to Mo–N as a cost-effective substitute of noble metals in hydrogenation catalyst applications (Dolce et al. 1997; Hargreaves 2013; Nagai 2007).

13.1.1 Hydrogenation (HYD)

Nitrogen inclusion significantly alters the catalytic activities of the host metal (Mo) by adjusting the bonding strengths and improving the electronic structure of the host (Oyama 1992). The higher catalytic activity and selectivity of TMNs than their metal hosts is ascribed to the electronic effect of metal nitrides, which is governed by the DOS of the *d*-orbital. In a nutshell, the metal–nitrogen bonds reduce the deficiency in the *d*-band occupancy of the metal,

promoting electron donations (Heine 1967) from the metallic to the N atoms. Owing to these significant electronic changes, the catalytic capacity of Mo–N based materials in hydrotreatment processes can match those of noble metals (Chen 1996; Chen et al. 2013b; Furimsky 2003).

The catalytic performance of transitional metal nitrides is highly sensitive to the selected transition metal, nitrogen ratio, and structural phase (cubic δ or hexagonal β). The δ phase generally affords a higher turnover frequency of β-Mo_2N than that in the hexagonal phase. Recent DFT studies have provided a molecular-level understanding of the catalytic reaction mechanisms over the surfaces of transitional metal nitrides. As mentioned earlier, NMR and TPD measurements provide insights into dissociative hydrogen adsorption on Mo_2N (Haddix et al. 1987; Li et al. 1996a, 1996b). The literature has reported the electronic factors contributing to catalysis over transitional metal nitrides and the governing mechanisms and surface modifications during the course of gaseous molecule–surface interactions. Nonetheless, several aspects warrant further investigation; most importantly, the phenomena leading to the poisoning of catalytic active sites at higher temperatures, the potential influences of dopants and atomic terminations on surface diffusion, and the effect of oxygen-rich streams versus pyrolytic conditions on catalytic activity.

Reviews on transitional metal nitrides have mainly summarized the structures and experimental findings related to hydroprocessing. TPD results pertinent to hydrogen interaction with Mo_2N have been discussed but without accounting for the mechanisms and structural/electronic factors contributing to the catalytic behaviour of TMNs. Selective HYDs are the core processes of many chemical industries. Furthermore, the HYD activity and/or the selectivity of TMNs is affected by several factors, including the SSA, nature of the surface-active sites, and crystalline phase of the catalyst (Nagai 2007).

Applying the DFT approach, Jaf et al. (2017) discussed the HYD of acetylene over catalysts assisted by γ-Mo_2N (100) and (111) indices. Consistent with the experimental observations, the proposed mechanism predicted a higher (lower) selectivity for the partial hydrogenation of acetylene to ethylene (ethane). Also consistent with the experiments, the irreversible mode of C_2H_2 over γ-Mo_2N demonstrated the exceptional catalytic properties of γ-Mo_2N in the selective hydrogenation of ethyne to ethene with a selectivity of 85% (Hao et al. 2000). The results of this investigation highlighted the promising industrial applications of crystalline metal nitride catalysts that selectively hydrogenate the triple bonds of ethyne to ethene. This selectivity primary stems from a higher activation barrier for the hydrogenation of alkenes in reference to their desorption. Our constructed mechanism by DFT calculations also shows a preference for the partial hydrogenation of 1,2-butadiene into C_4H_8 rather than full hydrogenation into C_4H1_0 (Jaf et al. 2018c). In other words, the selectivity toward partial hydrogenation stems from kinetic as well as thermodynamic considerations.

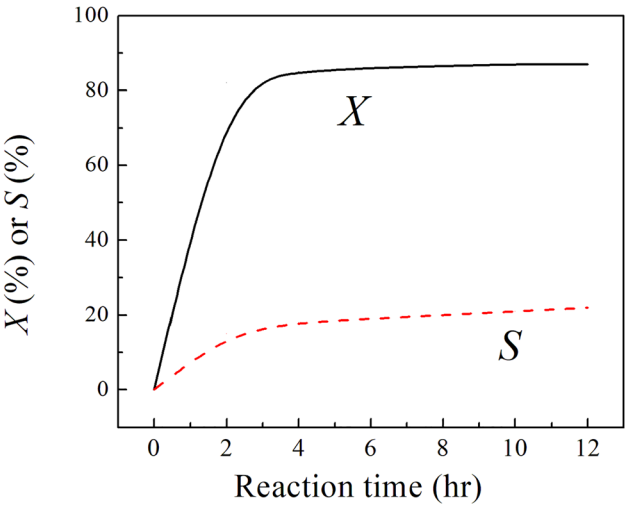

Figure 13: Temporal variation of acetylene conversion (X) and selectivity (S) of ethylene over γ-Mo_2N redrawn from Cárdenas-Lizana et al. (2018).

Recently, Cárdenas-Lizana et al. (2018) synthesized catalysts with two crystalline phases for the selective hydrogenation of alkyne: tetragonal β-Mo_2N with surface SSA = 6–15 $m^2\ g^{-1}$ and cubic γ-Mo_2N with SSA = 45–135 $m^2\ g^{-1}$. Catalytic tests disclosed that both materials were highly selective (77–90%) for acetylene hydrogenation to ethylene (see Figure 13).

13.1.2 Hydrodesulfurization (HDS)

Mo-based catalysts have been extensively deployed in the HDS of petroleum feed stocks. The HDS process eliminates the heteroatoms from thiophenic compounds such as thiophene, benzothiophene (BT), and dibenzothiophene (DBT) (Aegerter et al. 1996; Babich and Moulijn 2003; Markel and Van Zee 1990; McCrea et al. 1997; Nagai et al. 1993). The latter group of compounds are the major S-carriers in coals and transportation fuels. Ozkan et al. (1997) prepared an unsupported γ-Mo_2N catalyst for the HDS of BT in the presence/absence of NH_3. The catalyst was highly active toward ethylbenzene formation in the 473–653 temperature range.

To investigate the catalytic activity of DBT toward the HDS reaction, Park et al. (1997) prepared Co- and Ni-promoted nitrided Mo/γ-$A1_2O_3$ and unsupported molybdenum nitride catalysts by the TPR approach in an NH_3 environment. After carefully varying the temperature, pressure, and contact time, they increased the reactivity and selectivity of the catalysts in biphenyl (BPN) and cyclohexylbenzene (CHB) production. Liu et al. (2002) prepared γ-Mo_2N and Co-promoted molybdenum nitrides (Co–Mo–N) catalysts with high surface areas, and characterized them by XRD and BET. In the HDS of DBT, both γ-Mo_2N and Co–Mo–N exhibited higher HDS activity and selectivity for C–S bond rupture than C–H. Furthermore, the Co-promoter considerably enhanced the HDS activity of γ-Mo_2N. Supplementary Figure S8 depicts two main reaction corridors: the HYD of one aromatic ring into a mixture of 4H-DBT and 6H-DBT, which are rapidly converted to CHB by HDS, and the direct desulfurization of DBT to BPN by hydrogenolysis.

(Ramanathan and Oyama 1995) experimentally explored the catalytic activities of a series of transition metal carbides and nitrides of Mo, W, V, Nb, and Ti. The nitrides were prepared by TPR of their oxide precursors with a reactant gas (20% CH_4/H_2 for the carbide samples and 100% NH_3 for the nitride samples). BET chemisorption measurements were probed with N_2 and CO molecules. The HDN, HDS, and HDO activities of the catalysts were tested in a three-phase trickle-bed reactor. Supplementary Figure S9 compares the HDS activities of the studied catalysts. The commercial Ni–Mo/Al_2O_3 catalyst showed higher activity for DBT desulfurization than the transition metal carbides and nitrides. The catalytic activities of DBT desulfurization decreased in the order NiMo/Al_2O_3 > Mo_2C > WC > Mo_2N > NbC > VC > VN > TiN (i.e., group 6 > group 5 > group 4). Regardless of catalyst, benzene was the only distinguishable HDS product of DBT. The lower HDS activities of the carbides and nitrides may attributed to blockage of the available active sites by quinolone uptake. Mohammed et al. (2015) inspected the effect of Re metal on the activities of a Ni–Mo/γ-Al_2O_3 catalyst for sulfur removal from atmospheric gas oil as the temperature ranged from 275 to 350 °C under a pressure of 40 bar. Decoration with Re atoms improved the desulfurization activities of the Ni–Mo/γ-Al_2O_3 catalyst. The nitrogen-rich MoN_2 phase was found to be three times more effective in HDS reaction than the commonly utilized MoS_2 catalyst (Wang et al. 2015b). With the near-absence of N vacant sites in this N-rich phase, the mechanisms of HDS action could be distinctly different from these prevailing over the γ-Mo_2N surface. Our preliminary DFT calculations on HDS reactions over

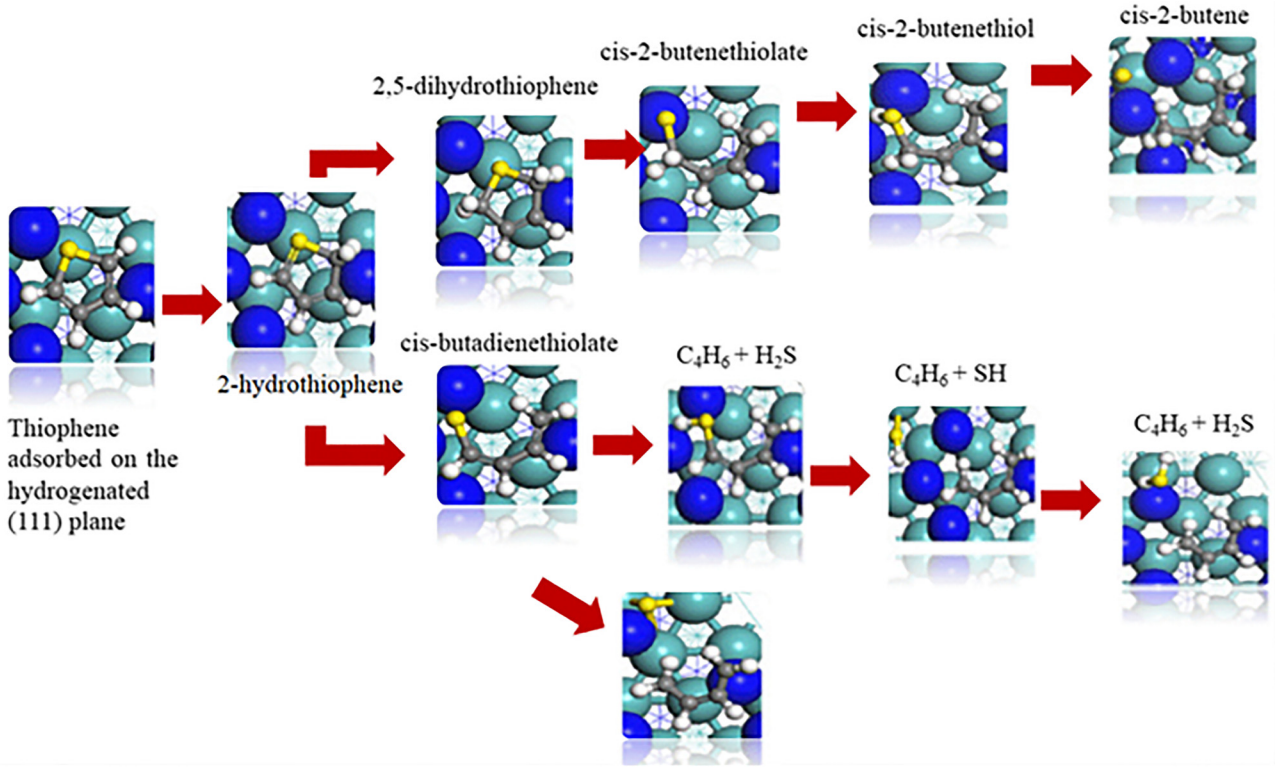

Figure 14: The proposed HDS reaction mechanism and geometries of thiophene over γ-Mo_2N surface redrawn from Jaf et al. (2018c).

the MoN_2 could not establish a feasible route that ensues via analogues mechanism to that established for the Mo_2N surface. Thus, it will be interesting to re-visit the HDS mechanism assisted by the MoN_2 surface.

Jaf et al. (2018c) emphasized the ability of molybdenum nitride catalysts to desulfurize simple aromatic molecules such as thiophene (C_4H_4S). They investigated the HDS mechanism of thiophene over γ-Mo_2N (111) slab by DFT. Thiophene was inferred to adsorb in a flat mode over the vacant 3-fold fcc sites. The HDS mechanism as depicted in Figure 14 ensues via complex pathways that mainly involve H transfer from the surface to the adsorbed thiophene, rupture of the C–S bond, surface hydrogenation of surface-bound S/SH adducts, and desorption of H_2S and cis-2-butene. We have found that the HDS route to entail lower activation energies than direct de-sulfurization.

13.1.3 Hydrogenation and de-chlorination of chloroamines

Transition metal nitrides promote the production of industrially important aromatic chloroamines (Dongil 2019). This topic is gaining traction in the catalyst fields. Of particular interest is the selective hydrogenation of *p*-CNB to *p*-CAN. The latter assumes direct applications in prominent chemical industries such as pharmaceuticals, polymers and pesticides. The hydrodechlorination of *p*-CNB to *p*-CAN comprises two primary reaction routes forming several intermediates (see Figure 15) (Jaf et al. 2018a). Along the direct pathway, the HYD of *p*-CNB generates chloronitrosobenzene and chlorophenylhydroxylamine as reaction by-products. A further hydrogen transfer reaction yields *p*-CAN. This condensation pathway forms nitroso and hydroxylamine intermediates that produce several side products, such as chloroazobenzene and chlorohydrazobenzene, which are subsequently hydrogenated to *p*-CAN (Jaf et al. 2018a).

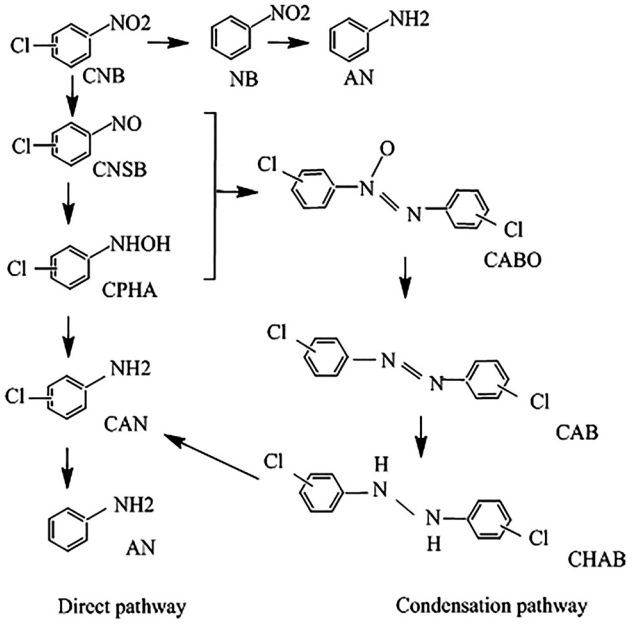

Figure 15: Reaction pathways in the hydrogenation of *p*-CNB to *p*-CAN. CNSB: chloronitrosobenzene, CPHA: chlorophenylhydroxylamine, CAB: chloroazobenzene, and CHAB: chlorohydrazobenzene, redrawn from Jaf et al. (2018a).

Several catalyst systems are selective for desired haloamines, including MgF_2/Ru–Cu catalysts (Pietrowski et al. 2011), Pd catalysts (Cárdenas-Lizana et al. 2013), activated carbon-supported Pt (Pt/AC) and Fe-promoted Pt (Pt–Fe/AC) catalysts (Chen et al. 2017), Au_{13} and Au_{55} nanoclusters (Zhang et al. 2018), and Ni/TiO_2 (Meng et al. 2010). Jujjuri et al. (2014) investigated the surface-mediated hydrochlorination (HDC) of 1,3-dichlorobenzene (1,3-DCB) They found that Ni/SiO_2 favored the concerted removal of both Cl substituents, producing a benzene molecule. Wang et al. (2017) fabricated a nanostructured δ-MoN catalyst with an onion-like morphology for the selective hydrogenation of functionalized nitroarene compounds. Jaf et al. (2018a) reported the selectivity of the γ-Mo_2N system for the HDC of aromatic molecules by probing the reduction mechanisms of *p*-CNB to *p*-CAN. Furthermore, DFT calculations of *p*-CNB showed a preference for two adsorption sites: Mo-hollow *fcc* and N-hollow *hcp*. The direct reduction of *p*-CNB to *p*-CAN via a chloronitrobenzene intermediate appeared to be the most preferred route. The primary steps in the constructed mechanism signifies H-transfer reactions from hollow sites to the NO/–NH groups via accessible reaction barriers followed by water elimination. Formulated thermo-kinetic model follows the reaction sequence shown in Figure 15 and elucidate the selectivity toward the hydrogenation cycle toward the experimentally observed products followed by water elimination steps. Most importantly, we have shown that direct de-chlorination through fission of the aromatic C–Cl bond to be unfeasible step. Overall, the hydrogenation of *p*-CNB by the Mo_2N surface was comparable to that of the Pd/ZnO (Cárdenas-Lizana et al. 2013).

13.1.4 Hydrodenitrogenation (HDN)

At present, hydrogenolysis of aromatic and nonaromatic hydrocarbons is the primary strategy for producing environmentally friendly fuels with no heteroatomic contents, most notably, S and N. This strategy requires cost-effective

catalysts that resist rapid activations and are catalytically efficient for HYD (Perot 1991; Rase 2016). Early studies reported the catalytic performance of high-surface-area transition metal carbides, nitrides, and borides for quinoline HDN in a batch autoclave reactor (Schlatter et al. 1988). The molybdenum carbide and nitride catalysts most effectively removed the N content from quinolone, with lower hydrogen consumption than the commercial Ni–Mo/$A1_2O_3$ catalyst. The structural sensitivity (i.e., the site density n, examined via CO chemisorption) minimally affected the catalytic activity of HDN and HDS reactions. Supplementary Figure S10 compares the quinoline HDN activities of carbides and nitrides with that of $NiMo/Al_2O_3$ at 643 K and 3.1 MPa. The HDN activity of Mo_2C was clearly comparable with that of a commercial $NiMo/Al_2O_3$ catalyst. The identified products of quinoline HDN were hydrogenated quinoline compounds and denitrogenated hydrocarbons (Ramanathan and Oyama 1995).

Lee et al. (1993) proposed the reaction routes of nitrogen removal from quinolone over the Mo_2N surface. Quinoline HDN was highly selective for the formation of propylbenzene from 1,2,3,4-tetrahydroquinoline and disfavored the formation of propylcyclohexane from decahydroquinoline. Senzi and Lee (1998) reported the HDN capacity of indole over a Mo_2N catalyst. The Mo_2N exhibited higher activity toward the HDN of indole than MoNi/γ-Al_2O_3 and consumed less hydrogen. The major reaction products of pyridine HDN over γ-Mo_2N are alkanes and pentane (Choi et al. 1992). Li et al. (1999) reported low H_2 consumption and high catalytic performance (activity and selectivity) of indole over *fcc*-Mo_2N prepared using the TPR method. They also synthesized *hcp*-Mo_2C via a sonochemical method. It was concluded that the structure, composition, and crystallinity of the catalysts are crucial in their activity and selectivity for indole HDN.

It has conveyed that Mo_2N activity greatly depends on the surface structure and availability of the active phases, which are distinguished as metallic Mo (modest-activity sites) and N deficient (high-activity sites) (Nagai 2007). Furthermore, catalytic performances of nitride catalysts for the hydrogenation reaction of carbazole HDN have been reported (Nagai et al. 2000). Nagai and Miyao (1992) demonstrated higher carbazole HDN activity in an alumina-supported molybdenum nitride catalyst than on sulfided and reduced phases at 553–633 K and 10.1 MPa total pressure. Chen et al. (2004) studied the catalytic decomposition of hydrazine (N_2H_4) over fresh and reduced passivated Mo_2N catalysts. They suggested that N_2H_4 is mainly adsorbed on the Mo sites. At a nitriding temperature of 700 K or lower, hydrazine fragments into NH_3 and N_2. At higher temperatures, NH_3 decomposes into hydrogen and nitrogen. Similar products were observed over Ir/γ-Al_2O_3 catalysts. Recently, Perret et al. (2019) showed contrasting effects of the Mo/N ratio on HYD and hydrogenolysis reactions. They postulated that the Mo/N ratio depends on the duration of Mo nitridation. Increasing the Mo/N ratio increased both the HYD rate of nitrobenzene with 100% selectivity to aniline and the hydrogenolysis rate of benzaldehyde to toluene.

13.1.5 Hydrodeoxygenation (HDO)

The HDO reaction of oxygen-containing structural entities has been successfully implemented on commercial scales by petrochemical industries (Furimsky 2000; Şenol et al. 2005). Ghampson et al. (2012) investigated how the nitriding procedure and support affect the properties of guaiacol HDO over molybdenum nitride catalysts. The Mo–N catalyst synthesized from an N_2/H_2 mixture through ammonolysis routes was more active for HDO than the catalysts synthesized by other routes owing to higher dispersion of the molybdenum oxynitride phase.

In another study, the same group reported that nonpromoted Mo_2N catalysts with the highest N/Mo concentration afford the maximum activity for guaiacol HDO (Ghampson et al. 2012). Furthermore, the HDO activity of guaiacol over alumina- and silica-supported molybdenum nitride catalysts was reported. The alumina-supported nitrides afforded a significant conversion of guaiacol to catechol, whereas the silica-supported catalysts achieved the highest phenol production with little catechol (Ghampson et al. 2012). Figure 16 shows the proposed reaction mechanism of guaiacol HDO over Mo_2N supported on commercial activated carbons. As shown in the figure, phenol and catechol were the most abundant products (Sepúlveda et al. 2011).

In a related study, Monnier et al. (2010) contrasted the catalytic activity of nitrides of molybdenum, tungsten and vanadium supported on α-Al_2O_3 toward HDO of oleic acid and canola oil. The alumina-supported metal nitrides catalysts were prepared by temperature programmed reaction with ammonia. The HDO reactions were carried out at relatively low temperatures of 380–410 °C under a 7.15 MPa flow of hydrogen. It was found that the HDO capacity of molybdenum nitride/Al_2O_3 clearly outperforms that of tungsten nitride/Al_2O_3, and vanadium/Al_2O_3 in terms of removal of oxygen, yields of normal alkanes, and

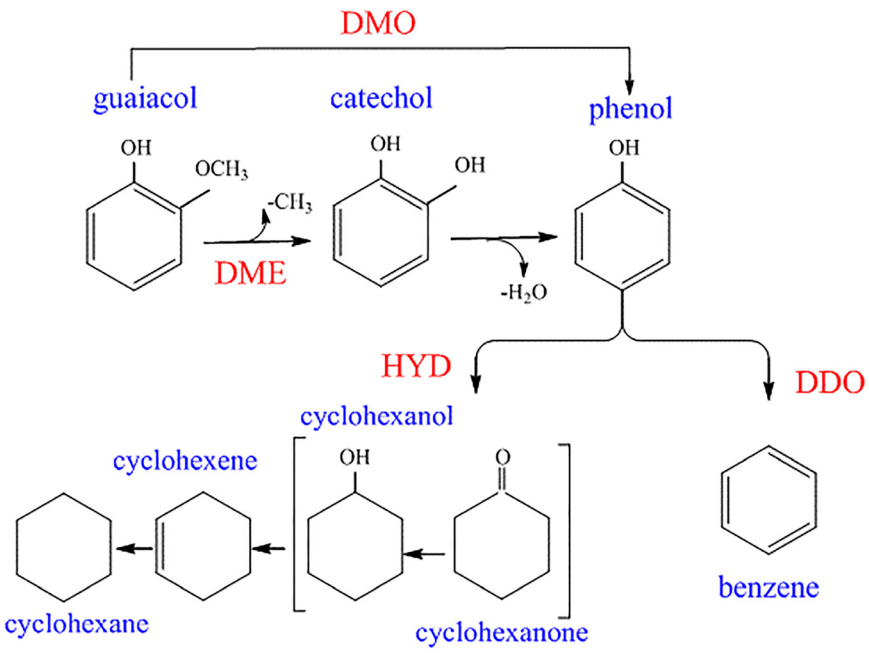

Figure 16: Reactions of guaiacol HDO proposed by Sepúlveda et al. (2011), reproduced with permission from Elsevier.

conversion of fatty acid. More importantly, the supported molybdenum nitride catalyst exhibited a profound selectivity (i.e., 75%) toward the production of n-$C_{18}H_{38}$ rather than decarbonylation and decarboxylation. These HDO performance indicators also surpass analogous values reported recently for bi- metallic catalysts (CuNiMo/γ-Al_2O_3, CrNiMo/γ-Al_2O_3 and FeNiMo/γ-Al_2O_3) (Arun et al. 2021) but close to that of 0.2-$NiMoS_2$ catalyst (Burimsitthigul et al. 2021). The mechanism that dictates higher selectivity toward the formation of normal alkanes (i.e., diesel enhances) over molybdenum nitride, remains unclear. However, we envisage that adsorbed hydrogen atoms selectively attack the carboxylic group releasing short alcohols. The formed alkane chain is weakly adsorbed to the surface without the presence of O-functional group. Thus, further degradation by the catalyst is not severely limited. Such hypothesis warrants investigations by DFT calculations.

13.2 Hydrogen evolution reaction (HER)

Proficient hydrogen production through water electrolysis is the main theme of catalysis research (Gray 2009; Lewis and Nocera 2006; Mueller-Langer et al. 2007). A commercially sustainable production of H_2 from sunlight and H_2O requires light absorbers and electrocatalysts fabricated from inexpensive materials (McKone et al. 2013, 2014). The typical electrocatalytic systems for H_2 generation integrate noble metal (mainly Pt) catalysts owing to their superior activity, low over-potential, and fast kinetics for driving the HER (Balogun et al. 2015; Greeley et al. 2006). The commercial applicability of these catalysts is hindered by the high cost and limited availability of noble metals (Yang 2009). In addition to Pt-based catalysts, many non-noble metal compounds have been synthesized and characterized as catalyst supports or promoters for HER applications. Their examples are MoS_2 nanoparticles (Jaramillo et al. 2007), WC (Esposito et al. 2010), pyrene-functionalized nickel complexes (Tran et al. 2011), and various metal alloys such as Ni and Ni–Mo alloy (McKone et al. 2011). The catalytic performances of compounds containing molybdenum and tungsten nitride outrun those of precious metals in hydrocarbon hydrogenolysis (Choi et al. 1992). Chen et al. (2012) synthesized $NiMoN_x$/C nanosheets with high HER electrocatalytic activity. Biomass-derived electrocatalytic composites for hydrogen production have received considerable interest because the catalyst is fabricated from earth-abundant metals (i.e., molybdenum) and soybeans (a common high-protein biomass). One recently developed soybean-based catalyst is MoSoy which comprises a β-Mo_2C phase and an acid-proof γ-Mo_2N phase (Chen et al. 2013a). The MoSoy catalyst mediates the HER occurrence and has a duration of more than 500 h in a corrosive acidic solution. Supported on graphene sheets, the MoSoy catalyst attains extremely fast charge-transfer kinetics with an overall performance similar to that of Pt for hydrogen production. The MoSoy

catalyst confirms that as a novel synthesis procedure, the hybridization of transition metals with high-protein biomass yields potentially applicable materials for the emerging hydrogen economy. Chen et al. (2014) stated that W_2C–WN nanoparticles grown on graphene nanoplates improve the HER efficiency. Graphene-supported W_2C and WN reduced the over-potential to nearly 120 mV at a current density of 10 mA/cm, whereas bulk W_2C catalyst required 336 mV at the same current density. In a recent review, Theerthagiri et al. (2020) reported that nitrides such as Ni, Ir, Ti, V, W, and Mo demonstrate efficient electrocatalytic activities for HER.

The water splitting reaction ($2H_2O \rightarrow 2H_2 + O_2$, $\Delta E = -1.23$ V) actually involves two reactions: the HER: $2H^+ + 2e^- \rightarrow H_2$ and the oxygen evolution reaction (OER): $2H_2O \rightarrow 4H^+ + O_2 + 4e^-$. The easy occurrence of both reactions requires an efficient electro- or photocatalyst. Nanostructured metal nitrides are known as efficient and cheap catalysts for electrochemical water splitting (Balogun et al. 2017; Jin et al. 2018). TMNs have also been applied as the electrocatalysts in rechargeable Zn–air batteries (Yu et al. 2020). Zhang et al. (2020) suggested that a heterostructured support surface for a γ-Mo_2N/Pt catalyst plays a significant activation role on the reactant molecules in the water–gas shift reaction.

13.3 Ammonia synthesis and decomposition reactions

Ammonia is a potentially viable hydrogen carrier in hydrogen fuel cells. Therefore, the synthesis and decomposition of NH_3 have been extensively investigated from both fundamental and commercial perspectives (Erdemir and Dincer 2021). Ammonia synthesis is an important reaction in the industrial production of strategic chemicals; most notably, of feed stocks such as fertilizers and nitric acid derivatives (Powell and Rossnagel 1999). The opposite process (NH_3 decomposition) affords hydrogen molecules by an environmentally friendly process with no toxic CO emissions. Commercially, NH_3 is produced through the Haber process over a ruthenium (Ru) catalyst. The Haber process generally occurs under mild temperature, concentration, and pressure conditions (Erisman et al. 2008; Jennings 2013). In terms of cost and synthesis conditions, metal nitride catalysts are considered superior to Ru-based catalysts (Hargreaves 2014). The activation activities of metal nitride catalysts in NH_3 synthesis are comparable to those of noble metal N_2 (Bell and Torrente-Murciano 2016).

Tagliazucca et al. (2013) fabricated molybdenum-based catalysts from MoO_3 and NH_2 for the decomposition of NH_3 into hydrogen and nitrogen molecules. Catalytic-assisted NH_3 decomposition has been reported multiple times in the literature (Zheng et al. 2013). The morphology of molybdenum nitrides trivially affects their catalytic performance for NH_3 synthesis (Mckay 2008), implying that the nanorod forms of β-$Mo_2N_{0.78}$ and γ-Mo_2N exhibit similar activities. As previously stated, the dissociative decomposition of NH_3 predominates at the N-vacant sites. Similarly, Podila et al. (2016) reported the production of hydrogen molecules from NH_3 over Mo_2N and Co_3Mo_3N catalysts with high surface areas.

13.4 Reforming reactions

Dry (CO_2) reforming of methane (DRM) is important in both scientific and industrial sectors. This reaction converts CH_4 and CO_2 into a syngas (i.e., CO and H_2) with a low H_2/CO ratio:

$$CH_4 + CO_2 \rightarrow 2CO + 2H_2.$$

This reaction is performed over a wide range of catalysts, most notably Ni, Co, Rh, Ru, Pt, and Pd metals.

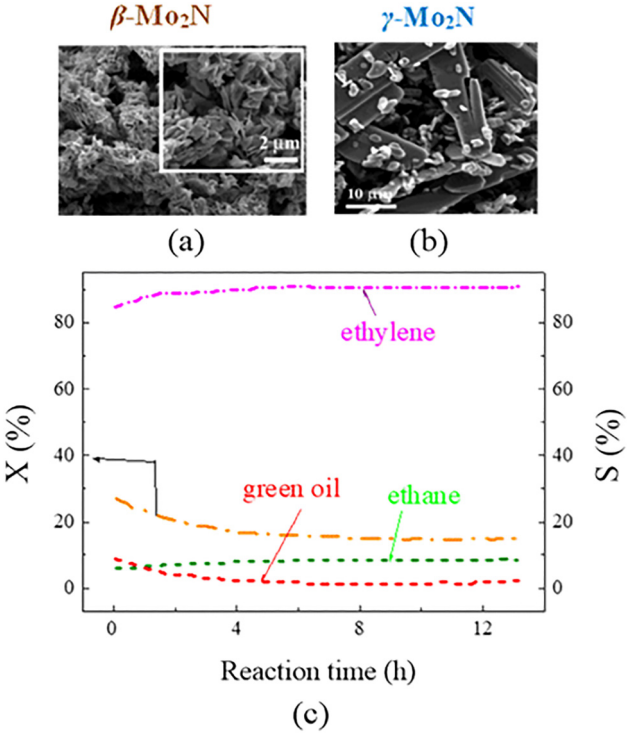

Figure 17: SEM images of fresh catalysts: (a) Mo_2N, (b) Ni_3Mo_3N, and (c) Co_3Mo_3N; (d) CH_4 and (e) CO_2 conversions for the dry reforming of methane over the Mo_2N, Ni_3Mo_3N, and Co_3Mo_3N catalysts (Fu et al. 2017), reproduced with permission from the Royal Society of Chemistry.

However, these catalysts are highly deactivated by carbon deposition, costly, and limited in availability. Commercial DRM processes require non-noble metal catalysts that resist carbon deposition. Although the effects of operating parameters on the syngas yield are adequately comprehended, the elementary steps of activating and converting the CH_4 and CO_2 remain highly speculative (Pakhare and Spivey 2014; Rostrupnielsen and Hansen 1993). Fu et al. (2017) synthesized nonprecious monometallic and bimetallic molybdenum nitrides-based catalysts for the DRM reaction. They found that Mo_2N, Ni_3Mo_3N, and Co_3Mo_3N cold catalyse the DRM reaction at temperatures beyond 550 °C. Moreover, the bimetallic nitrides Co_3Mo_3N and Ni_3Mo_3N showed higher catalytic activity, stability, and resistance to oxidation than molybdenum mononitride. Figure 17 shows SEM images of the fresh Mo_2N, Ni_3Mo_3N, and Co_3Mo_3N catalysts and plots their CH_4 and CO_2 conversions for the DRM as functions of temperature. The performance of the Co_3Mo_3N catalyst in regard to the very comparable yields of H_2 and CO is very close that of ceria–zirconia-supported nickel catalysts (Ni/CZ) (Radlik et al. 2015). Along the same line of enquiry, a higher methane/CO_2 conversion was obtained over the Co_3Mo_3N catalysts when compared to corresponding temperature-dependent conversion values over perovskites catalysts such as $Ir/\alpha\text{-}Al_2O_3 > Pd/\alpha\text{-}Al_2O_3 > Pt/\alpha\text{-}Al_2O_3$ (Bhattar et al. 2021).

However, it is also important to explore the fundamental aspects of the synergistic effect of introducing the Co/Ni into the lattice of Mo_2N. From the experimental study by Fu et al. (2017), it is evident that stand-alone Mo_2N catalyst does not activate the methane molecule, hence the exact role of the added could be limited to activation of the methyl C–H group. This is to be followed by selective degradation by the Mo_2N into CO and H_2. We propose that DRIFTS measurements coupled with DFT calculations could de-couple the effect of Ni/Co from that of Mo_2N. It is possible that addition of Ni/Co to enhance the concentrations of N vacant sites, and hence the surface hydrogenation of adsorbed methyl and carbonyl groups.

13.5 Oxygen reduction reaction (ORR) and methanol oxidation reaction (MOR)

Direct methanol fuel cells (DMFCs) are now recognized as a sustainable energy source. During the DMFC process, CO species are adsorbed through the electro-oxidation of methanol. Polar methanol molecules can diffuse through the membrane materials, gradually blocking the air electrode. Considerable efforts have been expended on catalysts that adsorb the produced CO molecules. The high cost incurred by Pt-based catalysts has hindered the commercialization of DMFCs. The development of innovative non-noble catalysts would substantially decrease the cost of DMFCs (Steele and Heinzel 2011).

Xia et al. (2008) produced a cost-effective MoN electrocatalyst with an approximate particle size of 4 nm. This catalyst, intended for oxygen reduction in DMFC applications, was fabricated via heat treatment of molybdenum tetraphenylporphyrin in an NH_3 atmosphere at different temperatures (600–1000 °C). In the electrochemical measurements, the synthesized MoN catalyst presented a durable oxidation reduction reaction (ORR) activity and was methanol tolerant. The structures of molybdenum nitrides are reportedly correlated with their catalytic activities toward the ORR and MOR. Qi et al. (2010) synthesized two carbon-supported molybdenum nitrides, MoN/C and Mo_2N/C, in an NH_3 environment and examined their catalytic activities for the ORR and MOR in O_2-saturated $HClO_4$ (0.5 M) and N_2-saturated 0.5 M $HClO_4$ (0.5 M) + CH_3OH (1.0 M) solutions, respectively. The stabilities of the MoN/C and Mo_2N/C catalysts in an oxygen atmosphere were confirmed through fast-scanning measurements in an O_2-saturated solution. The monometallic hexagonal molybdenum nitride (MoN/C) presented a higher activity than rock-salt-type molybdenum nitride (Mo_2N/C). This enhancement was ascribed either to the higher molybdenum valence or a more favorable coordination environment in the hexagonal phase. DFT calculations provided a molecular-level understanding of the structure–activity relationship in molybdenum nitrides (Qi et al. 2010). Both molybdenum nitride phases mediate the dissociation of O_2. An appropriately selected MoN configuration and preferential oxygen adsorption sites contribute to the high catalytic activity of MoN/C toward the ORR. Kreider et al. (2020) investigated the plausible correlation between O loads in the Mo–N configurations and the ORR activity. While a direct trend could not be established, it was postulated that N vacant sites facilitates O diffusion, and thus, electron transfer. Furthermore, they computed Gibbs free energies for the formation of random N vacant sites, without attempting to establish governing reaction pathways. In this regard, it is important to compute mass transfer coefficients and kinetic parameters for both ions transfers in order to fully understand the chemistry underlying ORR in MoN-based materials. Overall, Mo–N films exhibited a high activity with a selectivity to four-electron ORR comparable to that of Pt electrocatalysts (Sui et al. 2017).

Cao et al. (2015) synthesized several monometallic and bimetallic molybdenum nitrides by the ammonolysis of several precursors in the temperature range 600–750 °C. The prepared δ-MoN, Mo_5N_6, Mo_2N, and $Co_{0.6}Mo_{1.4}N_2$

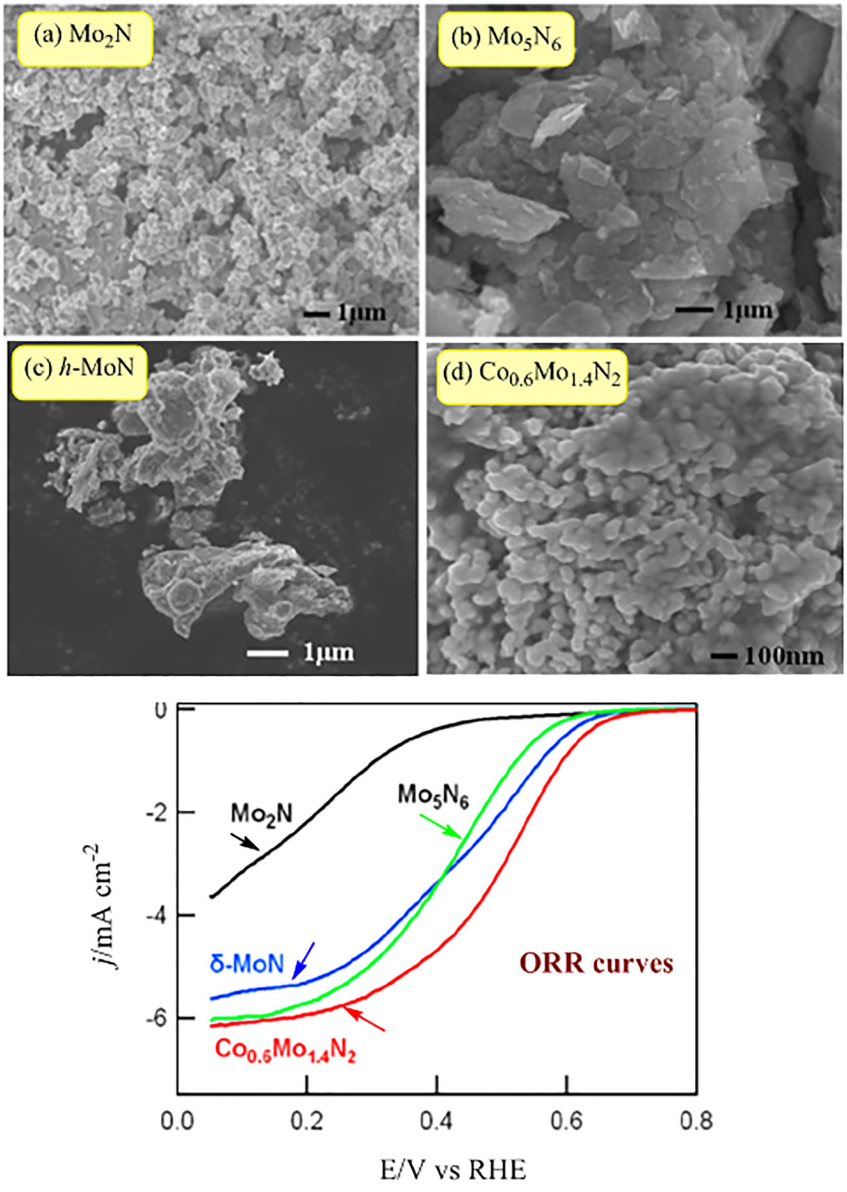

Figure 18: SEM images of Mo_2N, Mo_5N_6 and δ-MoN, and $Co_{0.6}Mo_{1.4}N_2$ nitrides (top) and their linear sweep voltammetry curves (bottom) (Cao et al. 2015), reproduced with permission from American Chemical Society.

phases were deployed as the ORR electrocatalysts in polymer electrolyte membrane fuel cells. The *fcc*–Mo_2N catalyst prepared from MoO_3 displayed poor ORR activity (E_{onset} = 0.420 V) in the acid electrolyte; however, the hexagonal δ-MoNs synthesized from $MoCl_5$ and Mo_5N_6 displayed higher ORR activities, as seen in Figure 18.

Spectrophotometric techniques have detected drug-containing amino groups, including mesalazine, metoclopramide, and dopamine, in pharmaceutical formulations based on ORR (Saleem 2019). It is worth mentioning that regulating the oxygen incorporation of surface and bulk MoN is essential for tailoring the catalytic performance of the ORR (Kreider et al. 2020). Furthermore, owing to their unique electronic structures, high conductivities, and good electro-catalytic activities, TMNs are important electrode materials in electrochemical energy-storage and conversion devices such as supercapacitors and rechargeable batteries (Dinh et al. 2019; Gao et al. 2019).

14 Conclusion and a future outlook

This review highlighted the structural configurations, synthesis procedures, and strategic catalytic and technological applications of mono-molybdenum nitrides. The surface area of the MoN_x phase (and hence its catalytic capacity) strongly depends on the synthesis conditions (the nitrogen precursors, heating and nitridation

temperature, and the flow rate). The mechanical properties of MoN_x strongly correlates with their N/M ratios where the microstructure switches from γ-Mo_2N to hexagonal and cubic MoN. With the variation in the degree of N saturation and evolution of the various phases, MoN_x configurations display a rather complex mixture of bonding states comprising covalent, metallic, and ionic characters. Owing to their high surface areas and vacant N sites, molybdenum nitrides are widely applied as stand-alone catalysts in hydrotreatment processes such as hydrogenation, hydrodesulfurization, hydrodenitrogenation, and hydrodeoxygenation. These operations eliminate hetero atoms such as N, S, O, and Cl from the fuel components. Furthermore, the potential roles of MoN-based materials as catalysts were comprehensively highlighted and discussed herein with a prime focus on the descried selectivity. Catalytic tests, surface characterizations techniques, and DFT calculations enabled to construct mechanisms for the surface-assisted action of MoN-based materials. Central in these mechanisms is the H transfer from the N vacant site to the adsorbed functional group. The formation of an oxide layer above the surface of MoN_x configurations seem to enhance their oxidation capacity via facilitating dissociative adsorption of water molecules. Decorating MoN-based materials with other atomic constituents assume a synergistic effect that entail activation of C–H bonds and hosting the dissociated adducts.

Having surveyed literature studies on applications of MoN-based materials, we envisage that future studies could focus on several aspects, most notably:

- The performance of bimetallic (Ni, Fe, Cu, Co) MoN--based catalysts in a wide array of catalytic applications requires further investigations. Literature presents a rather limited account on the catalytic capacity of these materials. The addition of another transition metal into the lattice of MoN may bring about a desired synergistic effect in HDO reactions, especially increasing the selectivity toward normal alkanes and suppressing further decomposition of the alkane chain.
- While literature present a detail mechanistic account of several surface-mediated reactions over MoN catalysts in light of experimental results, these postulated mechanisms remain without a kinetic proof. Elementary surface reactions could now be readily computed and complied into surface kinetic models. The model serves to survey variations in the occupied sites and the evolution of gas/aqueous phase products.
- Most literature studies on MoN-based catalysts have focused on HDO of oleic acids. Hydroxylated benzenes (such as vanillin) constitutes the largest fraction of oxygenated components in several types of bio-oil, such as these extracted from palm date trees. Thus, it will be important to assess the HDO capacity of MoN-based catalysts toward hydroxylated aromatics.
- The capacity of MoN-based materials in ORR applications stems from a facile movement of O anions through the N vacant sites. As such, it is essential to describe the associated electron transfer process with a prime objective to optimize the structural constituents in the MoN systems. The change in the oxidation states of Mo atoms during the electrochemical reactions can be traced by XPS analysis as well as by DFT calculations.
- The DFT-based stability diagram of Mo–N system in the literature could be extended to incorporate the effect various atomic dopants. More importantly, temperature/pressure-dependent thermo-mechanical properties could be evaluated against the fractional loads of these atomic dopants. This is essential to fine-tune the properties of the phase/configuration toward the desired applications in hard coatings or thermal insulations.
- The profound selective hydrogenation capacity of MoN-based catalysts calls for their deployment as hydrohalogenation catalysts with broad applications as environmental catalysts and in the treatment of halogenated species emitted during thermal recycling of e-waste. We envisage that N vacant sites could readily dissociate gas phase hydrogen halides with the subsequent formation of Cl_2/H_2. Clearly, such hypothesis necessitates experimental validation and DFT simulation to establish the working mechanism.

Nomenclature

1,3-DCB	1,3-dichlorobenzene
BET	Brunauer–Emmett–Teller (surface area)
BPN	biphenyl
BT	benzothiophene
CHB	cyclohexylbenzene
DBT	dibenzothiophene
DFT	density functional theory
DMFC	Direct methanol fuel cell
DOSs	density of states
DRM	dry reforming of methane
GGA	generalized gradient approximation
HER	hydrogen evolution reaction
HDC	hydrodechlorination
HDM	hydrodemetallization
HDN	hydrodenitrogenation

HDO	hydrodeoxygenation
HDS	hydrodesulfurization
HYD	hydrogenation
LHSV	liquid hourly space velocity
MOR	methanol oxidation reaction
NMR	nuclear magnetic resonance
OER	oxygen evolution reaction
p-CAN	*p*-chloroaniline
p-CAB	*p*-chloronitrobenzene
SSA	specific surface area
TMN	transition metal nitride
TPA	temperature programmed adsorption
TPD	temperature programmed desorption
TPR	temperature-programmed reaction
XPS	X-ray photoemission spectroscopy
XRD	X-ray diffraction

Acknowledgements: Z. J. and H. M. acknowledge the Iraqi Ministry of Higher Education and Scientific Research and University of Baghdad represented by the College of Education for Pure Sciences – Ibn Al-Haitham.

Author contributions: All the authors have accepted responsibility for the entire content of this submitted manuscript and approved submission.

Research funding: M. A. Acknowledges a UPAR grant from the United Arab Emirates University, grant ID: 31N451.

Conflict of interest statement: The authors declare no conflicts of interest regarding this article.

References

Abdelkader, H.S., Rabahi, A., Benaissa, M., and Benabadji, M.K. (2020). Theoretical investigation of structural and mechanical stability of Mo_2N. Solid State Commun. 314–315: 113919.

Aegerter, P.A., Quigley, W.W., Simpson, G.J., Ziegler, D.D., Logan, J.W., Mccrea, K.R., Glazier, S., and Bussell, M.E. (1996). Thiophene hydrodesulfurization over alumina-supported molybdenum carbide and nitride catalysts: adsorption sites, catalytic activities, and nature of the active surface. J. Catal. 164: 109–121.

Alexander, A.-M. and Hargreaves, J.S. (2010). Alternative catalytic materials: carbides, nitrides, phosphides and amorphous boron alloys. Chem. Soc. Rev. 39: 4388–4401.

Altarawneh, M., Jaf, Z., Oskierski, H., Jiang, Z.-T., Gore, J., and Dlugogorski, B.Z. (2016). Conversion of NO into N_2 over γ-Mo_2N. J. Phys. Chem. C 120: 22270–22280.

Arun, N., Nanda, S., Hu, Y., and Dalai, A.K. (2021). Hydrodeoxygenation of oleic acid using γ-Al_2O_3 supported transition metallic catalyst systems: insight into the development of novel FeCu/γ-Al_2O_3 catalyst. Mol. Catal.: 111526, https://doi.org/10.1016/j.mcat.2021.111526.

Babich, I. and Moulijn, J. (2003). Science and technology of novel processes for deep desulfurization of oil refinery streams: a review. Fuel 82: 607–631.

Baek, S.-H., Yun, K., Kang, D.-C., An, H., Park, M.B., Shin, C.-H., and Min, H.-K. (2021). Characteristics of high surface area molybdenum nitride and its activity for the catalytic decomposition of ammonia. Catalysts 11: 192.

Bafrali, R. and Bell, A.T. (1992). Interactions of H_2 and NH_3 with Mo (100) and Mo (100)-c (2×2) N surfaces. Surf. Sci. 278: 353–363.

Balasubramanian, K., Huang, L., and Gall, D. (2017). Phase stability and mechanical properties of $Mo_{1-x}N_x$ with $0 \le x \le 1$. J. Appl. Phys. 122: 195101.

Balasubramanian, K., Khare, S.V., and Gall, D. (2018). Energetics of point defects in rocksalt structure transition metal nitrides: thermodynamic reasons for deviations from stoichiometry. Acta Mater. 159: 77–88.

Balogun, M.-S., Huang, Y., Qiu, W., Yang, H., Ji, H., and Tong, Y. (2017). Updates on the development of nanostructured transition metal nitrides for electrochemical energy storage and water splitting. Mater. Today 20: 425–451.

Balogun, M.-S., Qiu, W., Wang, W., Fang, P., Lu, X., and Tong, Y. (2015). Recent advances in metal nitrides as high-performance electrode materials for energy storage devices. J. Mater. Chem. A 3: 1364–1387.

Bell, T.E. and Torrente-Murciano, L. (2016). H2 production via ammonia decomposition using non-noble metal catalysts: a review. Top. Catal. 59: 1438–1457.

Bezinge, A., Yvon, K., Muller, J., Lengaeur, W., and Ettmayer, P. (1987). High-pressure high-temperature experiments on δ-MoN. Solid State Commun. 63: 141–145.

Bhattar, S., Abedin, M.A., Kanitkar, S., and Spivey, J.J. (2021). A review on dry reforming of methane over perovskite derived catalysts. Catal. Today 365: 2–23.

Brewer, L. (1968). Bonding and structures of transition metals. Science 161: 115–122.

Bull, C.L., Kawashima, T., Mcmillan, P.F., Machon, D., Shebanova, O., Daisenberger, D., Soignard, E., Takayama-Muromachi, E., and Chapon, L.C. (2006). Crystal structure and high-pressure properties of γ-Mo_2N determined by neutron powder diffraction and X-ray diffraction. J. Solid State Chem. 179: 1762–1767.

Bull, C.L., Mcmillan, P.F., Soignard, E., and Leinenweber, K. (2004). Determination of the crystal structure of δ-MoN by neutron diffraction. J. Solid State Chem. 177: 1488–1492.

Burimsitthigul, T., Yoosuk, B., Ngamcharussrivichai, C., and Prasassarakich, P. (2021). Hydrocarbon biofuel from hydrotreating of palm oil over unsupported Ni–Mo sulfide catalysts. Renew. Energy 163: 1648–1659.

Butler, K.T., Sai Gautam, G., and Canepa, P. (2019). Designing interfaces in energy materials applications with first-principles calculations. npj Comput. Mater. 5: 19.

Cairns, A., Gallagher, J., Hargreaves, J., Mckay, D., Morrison, E., Rico, J., and Wilson, K. (2009). The influence of precursor source and thermal parameters upon the formation of beta-phase molybdenum nitride. J. Alloys Compd. 479: 851–854.

Cairns, A., Gallagher, J., Hargreaves, J., Mckay, D., Rico, J., and Wilson, K. (2010). The effect of low levels of dopants upon the formation and properties of beta-phase molybdenum nitride. J. Solid State Chem. 183: 613–619.

Calais, J.-L. (1977). Band structure of transition metal compounds. Adv. Phys. 26: 847–885.

Cao, B., Neuefeind, J.C., Adzic, R.R., and Khalifah, P.G. (2015). Molybdenum nitrides as oxygen reduction reaction catalysts: structural and electrochemical studies. Inorg. Chem. 54: 2128–2136.

Cardenas-Lizana, F., Gomez-Quero, S., Perret, N., Kiwi-Minsker, L., and Keane, M.A. (2011). β-molybdenum nitride: synthesis mechanism and catalytic response in the gas phase hydrogenation of *p*-chloronitrobenzene. Catal. Sci. Technol. 1: 794–801.

Cárdenas-Lizana, F., Hao, Y., Crespo-Quesada, M., Yuranov, I., Wang, X., Keane, M.A., and Kiwi-Minsker, L. (2013). Selective gas phase hydrogenation of p-chloronitrobenzene over Pd catalysts: role of the support. ACS Catal. 3: 1386–1396.

Cárdenas-Lizana, F., Lamey, D., Kiwi-Minsker, L., and Keane, M.A. (2018). Molybdenum nitrides: a study of synthesis variables and catalytic performance in acetylene hydrogenation. J. Mater. Sci. 53: 6707–6718.

Chen, H., He, D., He, Q., Jiang, P., Zhou, G., and Fu, W. (2017). Selective hydrogenation of p-chloronitrobenzene over an Fe promoted Pt/AC catalyst. RSC Adv. 7: 29143–29148.

Chen, J.G. (1996). Carbide and nitride overlayers on early transition metal surfaces: preparation, characterization, and reactivities. Chem. Rev. 96: 1477–1498.

Chen, W.-F., Iyer, S., Iyer, S., Sasaki, K., Wang, C.-H., Zhu, Y., Muckerman, J.T., and Fujita, E. (2013a). Biomass-derived electrocatalytic composites for hydrogen evolution. Energy Environ. Sci. 6: 1818–1826.

Chen, W.-F., Muckerman, J.T., and Fujita, E. (2013b). Recent developments in transition metal carbides and nitrides as hydrogen evolution electrocatalysts. Chem. Commun. 49: 8896–8909.

Chen, W.F., Sasaki, K., Ma, C., Frenkel, A.I., Marinkovic, N., Muckerman, J.T., Zhu, Y., and Adzic, R.R. (2012). Hydrogen-evolution catalysts based on non-noble metal nickel–molybdenum nitride nanosheets. Angew. Chem. Int. Ed. 51: 6131–6135.

Chen, W.F., Schneider, J.M., Sasaki, K., Wang, C.H., Schneider, J., Iyer, S., Iyer, S., Zhu, Y., Muckerman, J.T., and Fujita, E. (2014). Tungsten carbide–nitride on graphene nanoplatelets as a durable hydrogen evolution electrocatalyst. ChemSusChem 7: 2414–2418.

Chen, X., Zhang, T., Zheng, M., Wu, Z., Wu, W., and Li, C. (2004). The reaction route and active site of catalytic decomposition of hydrazine over molybdenum nitride catalyst. J. Catal. 224: 473–478.

Choi, D. and Kumta, P.N. (2011). Synthesis and characterization of nanostructured niobium and molybdenum nitrides by a two-step transition metal halide approach. J. Am. Ceram. Soc. 94: 2371–2378.

Choi, J.-G., Brenner, J.R., Colling, C.W., Demczyk, B.G., Dunning, J.L., and Thompson, L.T. (1992). Synthesis and characterization of molybdenum nitride hydrodenitrogenation catalysts. Catal. Today 15: 201–222.

Choi, J.-G., Curl, R.L., and Thompson, L.T. (1994). Molybdenum nitride catalysts: I. Influence of the synthesis factors on structural properties. J. Catal. 146: 218–227.

Claridge, J.B., York, A.P., Brungs, A.J., and Green, M.L. (2000). Study of the temperature-programmed reaction synthesis of early transition metal carbide and nitride catalyst materials from oxide precursors. Chem. Mater. 12: 132–142.

Colling, C.W., Choi, J.-G., and Thompson, L.T. (1996). Molybdenum nitride catalysts: II. H2 temperature programmed reduction and NH3 temperature programmed desorption. J. Catal. 160: 35–42.

Ding, L.-P., Shao, P., Zhang, F.-H., Lu, C., and Huang, X.-F. (2018). Prediction of molybdenum nitride from first-principle calculations: crystal structures, electronic properties, and hardness. J. Phys. Chem. C 122: 21039–21046.

Dinh, K.N., Liang, Q., Du, C.-F., Zhao, J., Tok, A.I.Y., Mao, H., and Yan, Q. (2019). Nanostructured metallic transition metal carbides, nitrides, phosphides, and borides for energy storage and conversion. Nano Today 25: 99–121.

Dolce, G., Savage, P., and Thompson, L. (1997). Hydrotreatment activities of supported molybdenum nitrides and carbides. Energy Fuels 11: 668–675.

Dongil, A. (2019). Recent progress on transition metal nitrides nanoparticles as heterogeneous catalysts. Nanomaterials 9: 1111.

Eichler, A. (2002). CO oxidation on transition metal surfaces: reaction rates from first principles. Surf. Sci. 498: 314–320.

Erdemir, D. and Dincer, I. (2021). A perspective on the use of ammonia as a clean fuel: challenges and solutions. Int. J. Energy Res. 45: 4827–4834.

Erisman, J.W., Sutton, M.A., Galloway, J., Klimont, Z., and Winiwarter, W. (2008). How a century of ammonia synthesis changed the world. Nat. Geosci. 1: 636.

Esposito, D.V., Hunt, S.T., Stottlemyer, A.L., Dobson, K.D., Mccandless, B.E., Birkmire, R.W., and Chen, J.G. (2010). Low-cost hydrogen-evolution catalysts based on monolayer platinum on tungsten monocarbide substrates. Angew. Chem. Int. Ed. 49: 9859–9862.

Ettmayer, P. (1970). Das system Molybdän-Stickstoff. Monatsh. Chem. 101: 127–140.

Frapper, G., Pélissier, M., and Hafner, J. (2000). CO Adsorption on molybdenum nitride's γ-Mo_2N (100) surface: formation of NCO species? A density functional study. J. Phys. Chem. B 104: 11972–11976.

Fu, X., Su, H., Yin, W., Huang, Y., and Gu, X. (2017). Bimetallic molybdenum nitride Co_3Mo_3N: a new promising catalyst for CO_2 reforming of methane. Catal. Sci. Technol. 7: 1671–1678.

Furimsky, E. (2000). Catalytic hydrodeoxygenation. Appl. Catal. Gen. 199: 147–190.

Furimsky, E. (2003). Metal carbides and nitrides as potential catalysts for hydroprocessing. Appl. Catal. Gen. 240: 1–28.

Ganin, A.Y., Kienle, L., and Vajenine, G.V. (2006). Synthesis and characterisation of hexagonal molybdenum nitrides. J. Solid State Chem. 179: 2339–2348.

Gao, B., Li, X., Ding, K., Huang, C., Li, Q., Chu, P.K., and Huo, K. (2019). Recent progress in nanostructured transition metal nitrides for advanced electrochemical energy storage. J. Mater. Chem. A 7: 14–37.

Gassner, G., Mayrhofer, P., Kutschej, K., Mitterer, C., and Kathrein, M. (2006). Magnéli phase formation of PVD Mo–N and W–N coatings. Surf. Coating. Technol. 201: 3335–3341.

Ghampson, I.T., Sepúlveda, C., Garcia, R., Radovic, L.R., Fierro, J.G., Desisto, W.J., and Escalona, N. (2012). Hydrodeoxygenation of guaiacol over carbon-supported molybdenum nitride catalysts: effects of nitriding methods and support properties. Appl. Catal. Gen. 439: 111–124.

Giordano, C. and Antonietti, M. (2011). Synthesis of crystalline metal nitride and metal carbide nanostructures by sol–gel chemistry. Nano Today 6: 366–380.

Gogotsi, Y.G. and Andrievski, R.A. (2012). Materials science of carbides, nitrides and borides. Springer Science & Business Media, Heidelberg, Germany.

Goldschmid, H.J. (2013). Interstitial alloys. Springer, Berlin, Germany.
Gray, H.B. (2009). Powering the planet with solar fuel. Nat. Chem. 1: 7.
Greczynski, G., Primetzhofer, D., Lu, J., and Hultman, L. (2017). Core-level spectra and binding energies of transition metal nitrides by non-destructive X-ray photoelectron spectroscopy through capping layers. Appl. Surf. Sci. 396: 347–358.
Greeley, J., Nørskov, J.K., Kibler, L.A., El-Aziz, A.M., and Kolb, D.M. (2006). Hydrogen evolution over bimetallic systems: understanding the trends. ChemPhysChem 7: 1032–1035.
Gregory, D.H. (1999). Structural families in nitride chemistry. J. Chem. Soc, Dalton Trans. 1: 259–270.
Guy, K., Tessier, F., Kaper, H., Grasset, F., Dumait, N., Demange, V., Nishio, M., Matsushita, Y., Matsui, Y., Takei, T., et al. (2020). Original synthesis of molybdenum nitrides using metal cluster compounds as precursors: applications in heterogeneous catalysis. Chem. Mater. 32: 6026–6034.
Haddix, G., Jones, D., Reimer, J., and Bell, A. (1988). Characterization of NH_3 adsorbed on γ-Mo_2N by NMR spectroscopy. J. Catal. 112: 556–564.
Haddix, G., Reimer, J., and Bell, A. (1987). Characterization of H_2 adsorbed on γ-Mo_2N by NMR spectroscopy. J. Catal. 108: 50–54.
Hägg, G. (1931). Gesetzmässigkeiten im Kristallbau bei Hydriden, Boriden, Carbiden und Nitriden der Übergangselemente. Z. Phys. Chem. 12: 33–56.
Ham, D.J. and Lee, J.S. (2009). Transition metal carbides and nitrides as electrode materials for low temperature fuel cells. Energies 2: 873–899.
Hao, Z., Wei, Z., Wang, L., Li, X., Li, C., Min, E., and Xin, Q. (2000). Selective hydrogenation of ethyne on γ-Mo_2N. Appl. Catal. Gen. 192: 81–84.
Hargreaves, J. (2013). Heterogeneous catalysis with metal nitrides. Coord. Chem. Rev. 257: 2015–2031.
Hargreaves, J. (2014). Nitrides as ammonia synthesis catalysts and as potential nitrogen transfer reagents. Appl. Petrochem. Res. 4: 3–10.
He, H., Dai, H.X., Ngan, K.Y., and Au, C.T. (2001). Molybdenum nitride for the direct decomposition of NO. Catal. Lett. 71: 147–153.
Heine, V. (1967). s– d interaction in transition metals. Phys. Rev. 153: 673.
Hillis, M., Kemball, C., and Roberts, M. (1966). Synthesis of ammonia and related processes on reduced molybdenum dioxide. Trans. Faraday Soc. 62: 3570–3585.
Höchst, H., Bringans, R., Steiner, P., and Wolf, T. (1982). Photoemission study of the electronic structure of stoichiometric and substoichiometric TiN and ZrN. Phys. Rev. B 25: 7183.
Hones, P., Martin, N., Regula, M., and Lévy, F. (2003). Structural and mechanical properties of chromium nitride, molybdenum nitride, and tungsten nitride thin films. J. Phys. D Appl. Phys. 36: 1023.
Hume-Rothery, W. (1968). The Engel-Brewer theories of metals and alloys. Prog. Mater. Sci. 13: 229–265.
Hunter, S.M., Mckay, D., Smith, R.I., Hargreaves, J.S., and Gregory, D.H. (2010). Topotactic nitrogen transfer: structural transformation in cobalt molybdenum nitrides. Chem. Mater. 22: 2898–2907.
Inumaru, K., Baba, K., and Yamanaka, S. (2005). Synthesis and characterization of superconducting β-Mo_2N crystalline phase on a Si substrate: an application of pulsed laser deposition to nitride chemistry. Chem. Mater. 17: 5935–5940.
Inumaru, K., Baba, K., and Yamanaka, S. (2006a). Preparation of superconducting molybdenum nitride MoNx ($0.5 \le x \le 1$) films with controlled composition. Phys. B Condens. Matter 383: 84–85.
Inumaru, K., Baba, K., and Yamanaka, S. (2006b). Structural distortion and suppression of superconductivity in stoichiometric B1–MoN epitaxial thin films. Phys. Rev. B 73: 052504.
Isaev, E.I., Simak, S.I., Abrikosov, I., Ahuja, R., Vekilov, Y.K., Katsnelson, M., Lichtenstein, A., and Johansson, B. (2007). Phonon related properties of transition metals, their carbides, and nitrides: a first-principles study. J. Appl. Phys. 101: 123519.
Jaf, Z.N., Altarawneh, M., Miran, H.A., Almatarneh, M.H., Jiang, Z.-T., and Dlugogorski, B.Z. (2018a). Catalytic hydrogenation of p-chloronitrobenzene to *p*-Chloroaniline mediated by γ-Mo_2N. ACS Omega 3: 14380–14391.
Jaf, Z.N., Altarawneh, M., Miran, H.A., and Jiang, Z.-T. (2018b). Geometries, electronic properties and stability of molybdenum and tungsten nitrides low-index surfaces. Mater. Res. Express 5: 126402.
Jaf, Z.N., Altarawneh, M., Miran, H.A., Jiang, Z.-T., and Dlugogorski, B.Z. (2018c). Hydrodesulfurization of thiophene over γ-Mo_2N catalyst. Mol. Catal. 459: 21–30.
Jaf, Z.N., Altarawneh, M., Miran, H.A., Jiang, Z.-T., and Dlugogorski, B.Z. (2017). Mechanisms governing selective hydrogenation of acetylene over γ-Mo_2N surfaces. Catal. Sci. Technol. 7: 943–960.
Jaf, Z.N., Jiang, Z.-T., Altarawneh, M., and Miran, H.A. (2016). Thermo-elastic and optical properties of molybdenum nitride. Can. J. Phys. 94: 902–912.
Jaggers, C.H., Michaels, J.N., and Stacy, A.M. (1990). Preparation of high-surface-area transition-metal nitrides: molybdenum nitrides, Mo_2N and MoN. Chem. Mater. 2: 150–157.
Jaramillo, T.F., Jørgensen, K.P., Bonde, J., Nielsen, J.H., Horch, S., and Chorkendorff, I. (2007). Identification of active edge sites for electrochemical H_2 evolution from MoS_2 nanocatalysts. Science 317: 100–102.
Jauberteau, I., Bessaudou, A., Mayet, R., Cornette, J., Jauberteau, J.L., Carles, P., and Merle-Méjean, T. (2015). Molybdenum nitride films: crystal structures, synthesis, mechanical, electrical and some other properties. Coatings 5: 656–687.
Jehn, H. and Ettmayer, P. (1978). The molybdenum-nitrogen phase diagram. J. Less Common. Met. 58: 85–98.
Jennings, J.R. (2013). Catalytic ammonia synthesis: fundamentals and practice. Springer Science & Business Media, Heidelberg, Germany.
Jhi, S.-H., Ihm, J., Louie, S.G., and Cohen, M.L. (1999). Electronic mechanism of hardness enhancement in transition-metal carbonitrides. Nature 399: 132–134.
Jin, H., Liu, X., Vasileff, A., Jiao, Y., Zhao, Y., Zheng, Y., and Qiao, S.-Z. (2018). Single-crystal nitrogen-rich two-dimensional Mo_5N_6 nanosheets for efficient and stable seawater splitting. ACS Nano 12: 12761–12769.
Johansson, L.I. (1995). Electronic and structural properties of transition-metal carbide and nitride surfaces. Surf. Sci. Rep. 21: 177–250.
Joshi, S., Wang, Q., Puntambekar, A., and Chakrapani, V. (2017). Facile synthesis of large area two-dimensional layers of transition-metal nitride and their use as insertion electrodes. ACS Energy Lett. 2: 1257–1262.
Kanoun, M., Goumri-Said, S., and Jaouen, M. (2007). Structure and mechanical stability of molybdenum nitrides: a first-principles study. Phys. Rev. B 76: 134109.
Karam, R. and Ward, R. (1970). Preparation of.beta.-molybdenum nitride. Inorg. Chem. 9: 1385–1387,.

Kawashima, T., Takayama-Muromachi, E., and Mcmillan, P.F. (2007). High-pressure synthesis and crystal structure of γ-Mo_2N. Physica C 460: 651–652.

Khojier, K., Mehr, M.R.K., and Savaloni, H. (2013). Annealing temperature effect on the mechanical and tribological properties of molybdenum nitride thin films. J. Nanostruct. Chem. 3: 5.

Klimashin, F., Koutná, N., Euchner, H., Holec, D., and Mayrhofer, P. (2016). The impact of nitrogen content and vacancies on structure and mechanical properties of Mo–N thin films. J. Appl. Phys. 120: 185301.

Kojima, R. and Aika, K.-I. (2001). Molybdenum nitride and carbide catalysts for ammonia synthesis. Appl. Catal. Gen. 219: 141–147.

Koutná, N., Holec, D., Friak, M., Mayrhofer, P.H., and Šob, M. (2018). Stability and elasticity of metastable solid solutions and superlattices in the MoN–TaN system: first-principles calculations. Mater. Des. 144: 310–322.

Koutná, N., Holec, D., Svoboda, O., Klimashin, F.F., Friak, M., and Mayrhofer, P.H. (2016). Point defects stabilise cubic Mo–N and Ta–N. J. Phys. D Appl. Phys. 49: 375303.

Kreider, M.E., Stevens, M.B., Liu, Y., Patel, A.M., Statt, M.J., Gibbons, B.M., Gallo, A., Ben-Naim, M., Mehta, A., and Davis, R.C. (2020). Nitride or oxynitride? Elucidating the composition–activity relationships in molybdenum nitride electrocatalysts for the oxygen reduction reaction. Chem. Mater. 32: 2946–2960.

Lahmer, M.A. (2019). The effect of growth conditions and vacancies on the electronic and mechanical properties of cubic Mo_2N; a DFT study. Comput. Condens. Matter 21: e00405.

Lee, J.S. and Ham, D.J. (2003). Metal nitrides. In: Encyclopedia of catalysis. John Wiley & Sons, Hoboken, New Jersey, pp. 15–32.

Lee, J.-Y. and Park, J.-W. (1996). Diffusion barrier property of molybdenum nitride films for copper metallization. Jpn. J. Appl. Phys. 35: 4280.

Lee, K.S., Abe, H., Reimer, J., and Bell, A. (1993). Hydrodenitrogenation of quinoline over high-surface-area Mo_2N. J. Catal. 139: 34–40.

Lengauer, W. (2000). Transition metal carbides, nitrides, and carbonitrides. In: Handbook of ceramic hard materials. John Wiley & Sons, Hoboken, New Jersey, pp. 202–252.

Lengauer, W. (2005). Nitrides: transition metal solid-state chemistry. Wiley Online Library, Hoboken, New Jersey.

Lévy, F., Hones, P., Schmid, P., Sanjinés, R., Diserens, M., and Wiemer, C. (1999). Electronic states and mechanical properties in transition metal nitrides. Surf. Coating. Technol. 120: 284–290.

Levy, R. and Boudart, M. (1973). Platinum-like behavior of tungsten carbide in surface catalysis. Science 181: 547–549.

Lewis, N.S. and Nocera, D.G. (2006). Powering the planet: chemical challenges in solar energy utilization. Proc. Natl. Acad. Sci. U. S. A. 103: 15729–15735.

Li, S., Kim, W.B., and Lee, J.S. (1998). Effect of the reactive gas on the solid-state transformation of molybdenum trioxide to carbides and nitrides. Chem. Mater. 10: 1853–1862.

Li, S., Lee, J.S., Hyeon, T., and Suslick, K.S. (1999). Catalytic hydrodenitrogenation of indole over molybdenum nitride and carbides with different structures. Appl. Catal. Gen. 184: 1–9.

Li, W., Yan, X., Aberle, A.G., and Venkataraj, S. (2015). Effect of deposition pressure on the properties of magnetron-sputter-deposited molybdenum back contacts for CIGS solar cells. Jpn. J. Appl. Phys. 54: 08KC14.

Li, X.S., Chen, Y.X., Zhang, Y.J., Ji, C.X., and Xin, Q. (1996a). Temperature-programmed desorption and adsorption of hydrogen on Mo_2N. React. Kinet. Catal. Lett. 58: 391–396.

Li, X.S., Zhang, Y.J., Xin, Q., Ji, C.X., Miao, Y.F., and Wang, L. (1996b). Irreversible hydrogen uptake on Mo_2N catalyst. React. Kinet. Catal. Lett. 57: 177–182.

Lin, S.-Y. and Lai, Y.-S. (2014). Effect of nitrogen on the physical properties and work function of MoN_x cap layers on HfO_2 gate dielectrics. ECS J. Solid State Sci. Technol. 3: N161–N165.

Liu, D., Liu, Y., Zhou, T., Liu, C., and Que, G. (2003). In situ FTIR study of co hydrogenation on a molybdenum nitride catalyst. Prepr. Pap.-Am. Chem. Soc., Div. Fuel Chem. 48: 506.

Liu, Y., Liu, C., and Que, G. (2002). Hydrodesulfurization of dibenzothiophene over cobalt– molybdenum nitride catalysts. Energy Fuels 16: 531–535.

Liu, Z., Zhou, X., Gall, D., and Khare, S. (2014). First-principles investigation of the structural, mechanical and electronic properties of the NbO-structured 3d, 4d and 5d transition metal nitrides. Comput. Mater. Sci. 84: 365–373.

Luo, Y.-R. (2002). Handbook of bond dissociation energies in organic compounds. CRC Press, Boca Raton, Florida.

Marchand, R., Gouin, X., Tessier, F., and Laurent, Y. (1996). New routes to molybdenum nitrides and oxynitrides: preparation and characterization of new phases. In: The chemistry of transition metal carbides and nitrides. Springer, Berlin, Germany, pp. 252–270.

Marchand, R., Tessier, F., and Disalvo, F.J. (1999). New routes to transition metal nitrides: and characterization of new phases. J. Mater. Chem. 9: 297–304.

Markel, E. and Van Zee, J. (1990). Catalytic hydrodesulfurization by molybdenum nitride. J. Catal. 126: 643–657.

Mccrea, K.R., Logan, J.W., Tarbuck, T.L., Heiser, J.L., and Bussell, M.E. (1997). Thiophene hydrodesulfurization over alumina-supported molybdenum carbide and nitride catalysts: effect of Mo loading and phase. J. Catal. 171: 255–267.

Mcgee, R.C.V. and Thompson, L.T. (2020). Nature of acid-base sites on molybdenum nitride catalysts: effect of nitrogen and oxygen content. Appl. Catal. Gen. 605: 117777.

Mckay, D. (2008). *Catalysis over molybdenum containing nitride materials, PhD Thesis*. University of Glasgow, Glasgow, Scotland.

Mckone, J.R., Lewis, N.S., and Gray, H.B. (2013). Will solar-driven water-splitting devices see the light of day? Chem. Mater. 26: 407–414.

Mckone, J.R., Marinescu, S.C., Brunschwig, B.S., Winkler, J.R., and Gray, H.B. (2014). Earth-abundant hydrogen evolution electrocatalysts. Chem. Sci. 5: 865–878.

Mckone, J.R., Warren, E.L., Bierman, M.J., Boettcher, S.W., Brunschwig, B.S., Lewis, N.S., and Gray, H.B. (2011). Evaluation of Pt, Ni, and Ni–Mo electrocatalysts for hydrogen evolution on crystalline Si electrodes. Energy Environ. Sci. 4: 3573–3583.

Meng, X., Cheng, H., Fujita, S.-I., Hao, Y., Shang, Y., Yu, Y., Cai, S., Zhao, F., and Arai, M. (2010). Selective hydrogenation of chloronitrobenzene to chloroaniline in supercritical carbon dioxide over Ni/TiO_2: significance of molecular interactions. J. Catal. 269: 131–139.

Mitterer, C., Holler, F., Üstel, F., and Heim, D. (2000). Application of hard coatings in aluminium die casting—soldering, erosion and thermal fatigue behaviour. Surf. Coating. Technol. 125: 233–239.

Mohammed, A.H.A.K., Hussein, H.Q., and Naife, T.M. (2015). Comparative study of new Re-Ni-Mo/Al_2o_3 and conventional hydrodesulphurization catalyst. Iraqi J. Chem. Petrol. Eng. 16: 1–9.

Monnier, J., Sulimma, H., Dalai, A., and Caravaggio, G. (2010). Hydrodeoxygenation of oleic acid and canola oil over alumina-supported metal nitrides. Appl. Catal, A 382: 176–180.

Mueller-Langer, F., Tzimas, E., Kaltschmitt, M., and Peteves, S. (2007). Techno-economic assessment of hydrogen production processes for the hydrogen economy for the short and medium term. Int. J. Hydrogen Energy 32: 3797–3810.

Nagai, M. (2007). Transition-metal nitrides for hydrotreating catalyst — synthesis, surface properties, and reactivities. Appl. Catal. Gen. 322: 178–190.

Nagai, M. and Miyao, T. (1992). Activity of alumina-supported molybdenum nitride for carbazole hydrodenitrogenation. Catal. Lett. 15: 105–109.

Nagai, M., Miyao, T., and Tuboi, T. (1993). Hydrodesulfurization of dibenzothiophene on alumina-supported molybdenum nitride. Catal. Lett. 18: 9–14.

Nagai, M., Goto, Y., Irisawa, A., and Omi, S. (2000). Catalytic activity and surface properties of nitrided molybdena–alumina for carbazole hydrodenitrogenation. J. Catal. 191: 128–137.

Neylon, M., Choi, S., Kwon, H., Curry, K., and Thompson, L. (1999). Catalytic properties of early transition metal nitrides and carbides: n-butane hydrogenolysis, dehydrogenation and isomerization. Appl. Catal. Gen. 183: 253–263.

Oyama, S.T. (1992). Crystal structure and chemical reactivity of transition metal carbides and nitrides. J. Solid State Chem. 96: 442–445.

Oyama, S.T. (1996). Introduction to the chemistry of transition metal carbides and nitrides. In: The chemistry of transition metal carbides and nitrides. Springer, Berlin, Germany, pp. 1–27.

Ozkan, U.S., Zhang, L., and Clark, P.A. (1997). Performance and postreaction characterization of γ-Mo_2N catalysts in simultaneous hydrodesulfurization and hydrodenitrogenation reactions. J. Catal. 172: 294–306.

Pakhare, D. and Spivey, J. (2014). A review of dry (CO_2) reforming of methane over noble metal catalysts. Chem. Soc. Rev. 43: 7813–7837.

Papaconstantopoulos, D. and Pickett, W. (1985). Effects of disorder on high-temperature superconductivity in cubic MoN. Phys. Rev. B 31: 7093.

Papaconstantopoulos, D., Pickett, W., Klein, B., and Boyer, L. (1985). Electronic properties of transition-metal nitrides: the group-V and group-VI nitrides VN, NbN, TaN, CrN, MoN, and WN. Phys. Rev. B 31: 752.

Park, H.K., Lee, J.K., Yoo, J.K., Ko, E.S., and Kim, K.L. (1997). Surface properties and reactivity of supported and unsupported molybdenum nitride catalysts. Appl. Catal. Gen. 150: 21–35.

Perot, G. (1991). The reactions involved in hydrodenitrogenation. Catal. Today 10: 447–472.

Perret, N., Cárdenas-Lizana, F., Lamey, D., Laporte, V., Kiwi-Minsker, L., and Keane, M.A. (2012). Effect of crystallographic phase (β vs. γ) and surface area on gas phase nitroarene hydrogenation over Mo_2N and Au/Mo_2N. Top. Catal. 55: 955–968.

Perret, N., Lamey, D., Kiwi-Minsker, L., Cárdenas-Lizana, F., and Keane, M.A. (2019). New insights into the effect of nitrogen incorporation in Mo: catalytic hydrogenation vs. hydrogenolysis. Catal. Sci. Technol. 9: 1891–1901.

Pietrowski, M., Zieliński, M., and Wojciechowska, M. (2011). High-selectivity hydrogenation of chloronitrobenzene to chloroaniline over magnesium fluoride-supported bimetallic ruthenium-copper catalysts. ChemCatChem 3: 835–838.

Podila, S., Zaman, S.F., Driss, H., Alhamed, Y.A., Al-Zahrani, A.A., and Petrov, L.A. (2016). Hydrogen production by ammonia decomposition using high surface area Mo_2N and Co_3Mo_3N catalysts. Catal. Sci. Technol. 6: 1496–1506.

Powell, R.A. and Rossnagel, S. (1999). *PVD for microelectronics: sputter deposition applied to semiconductor manufacturing (thin films)*. Academic Press, London.

Qi, J., Jiang, L., Jiang, Q., Wang, S., and Sun, G. (2010). Theoretical and experimental studies on the relationship between the structures of molybdenum nitrides and their catalytic activities toward the oxygen reduction reaction. J. Phys. Chem. C 114: 18159–18166.

Radlik, M., Adamowska-Teyssier, M., Krztoń, A., Kozieł, K., Krajewski, W., Turek, W., and Da Costa, P. (2015). Dry reforming of methane over Ni/$Ce_{0.62}Zr_{0.38}O_2$ catalysts: effect of Ni loading on the catalytic activity and on H_2/CO production. Compt. Rendus Chem. 18: 1242–1249.

Ramanathan, S. and Oyama, S.T. (1995). New catalysts for hydroprocessing: transition metal carbides and nitrides. J. Phys. Chem. 99: 16365–16372.

Ranhotra, G., Haddix, G., Bell, A., and Reimer, J. (1987). Catalysis over molybdenum carbides and nitrides: I. Catalyst characterization. J. Catal. 108: 24–39.

Rase, H.F. (2016). Handbook of commercial catalysts: heterogeneous catalysts. CRC Press, Boca Raton, Florida.

Rostrupnielsen, J. and Hansen, J.B. (1993). CO_2-reforming of methane over transition metals. J. Catal. 144: 38–49.

Roy, A., Serov, A., Artyushkova, K., Brosha, E.L., Atanassov, P., and Ward, T.L. (2015). Facile synthesis of high surface area molybdenum nitride and carbide. J. Solid State Chem. 228: 232–238.

Saito, K. and Asada, Y. (1987). Superconductivity and structural changes of nitrogen-ion implanted Mo thin films. J. Phys. F Met. Phys. 17: 2273.

Saleem, B.A. (2019). Spectrophotometric determination of some drugs using oxidation reduction reactions. Ibn AL- Haitham J. Pure Appl. Sci. 32: 43–55.

Sangiovanni, D.G., Hultman, L., and Chirita, V. (2011). Supertoughening in B1 transition metal nitride alloys by increased valence electron concentration. Acta Mater. 59: 2121–2134.

Sanjinés, R., Wiemer, C., Almeida, J., and Levy, F. (1996). Valence band photoemission study of the Ti–Mo–N system. Thin Solid Films 290: 334–338.

Schlatter, J.C., Oyama, S.T., Metcalfe, J.E., III, and Lambert, J.M., Jr. (1988). Catalytic behavior of selected transition metal carbides, nitrides, and borides in the hydrodenitrogenation of quinoline. Ind. Eng. Chem. Res. 27: 1648–1653.

Şenol, O., Viljava, T.-R., and Krause, A. (2005). Hydrodeoxygenation of methyl esters on sulphided NiMo/γ-Al_2O_3 and CoMo/γ-Al_2O_3 catalysts. Catal. Today 100: 331–335.

Senzi, L. and Lee, J.S. (1998). Molybdenum nitride and carbide prepared from heteropolyacid: II. Hydrodenitrogenation of indole. J. Catal. 173: 134–144.

Sepúlveda, C., Leiva, K., García, R., Radovic, L., Ghampson, I., Desisto, W., Fierro, J.G., and Escalona, N. (2011). Hydrodeoxygenation of 2-methoxyphenol over Mo_2N catalysts supported on activated carbons. Catal. Today 172: 232–239.

Shen, Y. (2003). Effect of deposition conditions on mechanical stresses and microstructure of sputter-deposited molybdenum and reactively sputter-deposited molybdenum nitride films. Mater. Sci. Eng. A 359: 158–167.

Soignard, E., Mcmillan, P.F., Chaplin, T.D., Farag, S.M., Bull, C.L., Somayazulu, M.S., and Leinenweber, K. (2003). High-pressure synthesis and study of low-compressibility molybdenum nitride (MoN and MoN_{1-x}) phases. Phys. Rev. B 68: 132101.

Sproul, W.D. (1986). Reactively sputtered nitrides and carbides of titanium, zirconium, and hafnium. J. Vac. Sci. Technol, A 4: 2874–2878.

Stampfl, C. (2005). Surface processes and phase transitions from ab initio atomistic thermodynamics and statistical mechanics. Catal. Today 105: 17–35.

Steele, B.C. and Heinzel, A. (2011). Materials for fuel-cell technologies. In: Materials for sustainable energy: a collection of peer-reviewed research and review articles from Nature Publishing Group. World Scientific, Singapore, pp. 20–30.

Stevens, F., Carmichael, I., Callens, F., and Waroquier, M. (2006). Density functional investigation of high-spin XY (X = Cr, Mo, W and Y = C, N, O) molecules. J. Phys. Chem. A 110: 4846–4853.

Sui, S., Wang, X., Zhou, X., Su, Y., Riffat, S., and Liu, C.-J. (2017). A comprehensive review of Pt electrocatalysts for the oxygen reduction reaction: nanostructure, activity, mechanism and carbon support in PEM fuel cells. J. Mater. Chem. A 5: 1808–1825.

Sun, G.D., Zhang, G.H., and Chou, K.C. (2018). Synthesis of molybdenum nitrides nanosheets by nitriding 2H-MoS_2 with ammonia. J. Am. Ceram. Soc. 101: 2796–2808.

Sun, W., Holder, A., Orvañanos, B., Arca, E., Zakutayev, A., Lany, S., and Ceder, G. (2017). Thermodynamic routes to novel metastable nitrogen-rich nitrides. Chem. Mater. 29: 6936–6946.

Suszko, T., Gulbiński, W., and Jagielski, J. (2005). The role of surface oxidation in friction processes on molybdenum nitride thin films. Surf. Coating. Technol. 194: 319–324.

Tagliazucca, V., Schlichte, K., Schüth, F., and Weidenthaler, C. (2013). Molybdenum-based catalysts for the decomposition of ammonia: in situ X-ray diffraction studies, microstructure, and catalytic properties. J. Catal. 305: 277–289.

Theerthagiri, J., Lee, S.J., Murthy, A.P., Madhavan, J., and Choi, M.Y. (2020). Fundamental aspects and recent advances in transition metal nitrides as electrocatalysts for hydrogen evolution reaction: a review. Curr. Opin. Solid State Mater. Sci. 24: 100805.

Toth, L. (2014). Transition metal carbides and nitrides. Elsevier, Amsterdam, Netherlands.

Tran, P.D., Le Goff, A., Heidkamp, J., Jousselme, B., Guillet, N., Palacin, S., Dau, H., Fontecave, M., and Artero, V. (2011). Noncovalent modification of carbon nanotubes with pyrene-functionalized nickel complexes: carbon monoxide tolerant catalysts for hydrogen evolution and uptake. Angew. Chem. 123: 1407–1410.

Volpe, L. and Boudart, M. (1985). Compounds of molybdenum and tungsten with high specific surface area: I. Nitrides. J. Solid State Chem. 59: 332–347.

Wang, C., Akbar, S., Chen, W., and Patton, V. (1995). Electrical properties of high-temperature oxides, borides, carbides, and nitrides. J. Mater. Sci. 30: 1627–1641.

Wang, S., Antonio, D., Yu, X., Zhang, J., Cornelius, A.L., He, D., and Zhao, Y. (2015a). The hardest superconducting metal nitride. Sci. Rep. 5: 13733.

Wang, S., Ge, H., Sun, S., Zhang, J., Liu, F., Wen, X., Yu, X., Wang, L., Zhang, Y., and Xu, H. (2015b). A new molybdenum nitride catalyst with rhombohedral MoS_2 structure for hydrogenation applications. J. Am. Chem. Soc. 137: 4815–4822.

Wang, S., Ge, H., Han, W., Li, Y., Zhang, J., Yu, X., Qin, J., Quan, Z., Wen, X., and Li, X. (2017). Synthesis of onion-like δ-MoN catalyst for selective hydrogenation. J. Phys. Chem. C 121: 19451–19460.

Wang, Y. and Ding, Y. (2016). The hydrogen-induced structural stability and promising electronic properties of molybdenum and tungsten dinitride nanosheets: a first-principles study. J. Mater. Chem. C 4: 7485–7493.

Wang, Y., Li, J., and Wei, Z. (2018). Transition-metal-oxide-based catalysts for the oxygen reduction reaction. J. Mater. Chem. A 6: 8194–8209.

Wei, Q., Zhao, C., Zhang, M., Yan, H., and Wei, B. (2019). High-pressure phases and pressure-induced phase transition of MoN_6 and ReN_6. Phys. Lett. A 383: 2429–2435.

Wise, R. and Markel, E. (1994). Synthesis of high surface area molybdenum nitride in mixtures of nitrogen and hydrogen. J. Catal. 145: 344–355.

Xie, J., Li, S., Zhang, X., Zhang, J., Wang, R., Zhang, H., Pan, B., and Xie, Y. (2014). Atomically-thin molybdenum nitride nanosheets with exposed active surface sites for efficient hydrogen evolution. Chem. Sci. 5: 4615–4620.

Xia, D., Liu, S., Wang, Z., Chen, G., Zhang, L., Zhang, L., Hui, S.R., and Zhang, J. (2008). Methanol-tolerant MoN electrocatalyst synthesized through heat treatment of molybdenum tetraphenylporphyrin for four-electron oxygen reduction reaction. J. Power Sources 177: 296–302.

Xu, H., Zhang, H., Fang, L., Yang, J., Wu, K., and Wang, Y. (2015). Hierarchical molybdenum nitride nanochexes by a textured self-assembly in gas–solid phase for the enhanced application in lithium ion batteries. ACS Nano 9: 6817–6825.

Yang, C.-J. (2009). An impending platinum crisis and its implications for the future of the automobile. Energy Pol. 37: 1805–1808.

Yang, S., Li, C., Xu, J., and Xin, Q. (1998). Surface sites of alumina-supported molybdenum nitride characterized by FTIR, TPD-MS, and volumetric chemisorption. J. Phys. Chem. B 102: 6986–6993.

Yu, S., Huang, B., Jia, X., Zeng, Q., Oganov, A.R., Zhang, L., and Frapper, G. (2016). Exploring the real ground-state structures of molybdenum dinitride. J. Phys. Chem. C 120: 11060–11067.

Yu, X., Zhou, T., Ge, J., and Wu, C. (2020). Recent advances on the modulation of electrocatalysts based on transition metal nitrides for the rechargeable Zn-air battery. ACS Mater. Lett. 2: 1423–1434.

Zaman, S. (2010). A DFT study of CO adsorption and dissociation over γ-Mo_2N (111) plane. Bulg. Chem. Commun. 47: 125–132.

Zeinalipour-Yazdi, C.D., Hargreaves, J.S., and Catlow, C.R.A. (2015). Nitrogen activation in a Mars–van Krevelen mechanism for ammonia synthesis on Co_3Mo_3N. J. Phys. Chem. C 119: 28368–28376.

Zhang, Y., Li, Y., Li, C., and Xin, Q. (1997). Adsorption and migration of hydrogen on different surface sites of γ-Mo_2N catalyst. In: Studies in surface science and catalysis. Elsevier, Amsterdam, Netherlands, pp. 457–464.

Zhang, C., Liu, J., Shen, H., Li, X.-Z., and Sun, Q. (2017). Identifying the ground state geometry of a MoN_2 sheet through a global structure search and its tunable p-electron half-metallicity. Chem. Mater. 29: 8588–8593.

Zhang, L., Ni, Z., Xue, J., Qian, H., Liu, Y., and Jin, C. (2018). Selective hydrogenation of *p*-chloronitrobenzene on nanosized gold clusters: a theoretical study. Chem. Phys. Lett. 703: 23–28.

Zhang, S., Sun, D., Fu, Y., and Du, H. (2003). Recent advances of superhard nanocomposite coatings: a review. Surf. Coating. Technol. 167: 113–119.

Zhang, X., Yu, Z., Wang, S.-S., Guan, S., Yang, H.Y., Yao, Y., and Yang, S.A. (2016). Theoretical prediction of MoN_2 monolayer as a high capacity electrode material for metal ion batteries. J. Mater. Chem. A 4: 15224–15231.

Zhang, Z.-S., Fu, Q., Xu, K., Wang, W.-W., Fu, X.-P., Zheng, X.-S., Wu, K., Ma, C., Si, R., and Jia, C.-J. (2020). Intrinsically active surface in a Pt/γ-Mo_2N catalyst for the water–gas shift reaction: molybdenum nitride or molybdenum oxide? J. Am. Chem. Soc. 142: 13362–13371.

Zhao, E., Wang, J., Meng, J., and Wu, Z. (2010). Structural, mechanical and electronic properties of 4d transition metal mononitrides by first-principles. Comput. Mater. Sci. 47: 1064–1071.

Zhao, X. and Range, K.-J. (2000). High pressure synthesis of molybdenum nitride MoN. J. Alloys Compd. 296: 72–74.

Zheng, W., Cotter, T.P., Kaghazchi, P., Jacob, T., Frank, B., Schlichte, K., Zhang, W., Su, D.S., Schüth, F., and Schlögl, R. (2013). Experimental and theoretical investigation of molybdenum carbide and nitride as catalysts for ammonia decomposition. J. Am. Chem. Soc. 135: 3458–3464.

Supplementary Material: The online version of this article offers supplementary material (https://doi.org/10.1515/revce-2021-0002).